Electric Field Poling in Polymeric Nonlinear Optical Materials. Relaxation Dynamics, Model, and Experiment

Millicent A. Firestone,‡ Mark A. Ratner,* and Tobin J. Marks*

Department of Chemistry and the Materials Research Center, Northwestern University, Evanston, Illinois 60208-3113

Received January 31, 1995; Revised Manuscript Received May 30, 1995®

ABSTRACT: Simulations of the electric field poling process for second-order NLO-active polymeric materials containing dipolar chromophores were performed by modeling the time-dependent dynamics of a dipole interacting with an externally applied field and subsequent force-free relaxation, employing several modifications of the Smoluchowski equation. The model examines chromophore dipole alignment/relaxation processes in both two- and three-dimensional space. The 3-D model predicts that at field-on equilibrium, the ratio, R, of the second-harmonic coefficients, d_{33}/d_{31}, approaches 3.0, in accord with static statistical−mechanical models. In contrast, the 2-D model predicts $R \sim 6.0$. The dimensionality in which the rotational diffusion process is confined also determines the rate of dipolar alignment/relaxation, with a slower rate predicted in the 2-D case. Suitability of the rotational diffusion model for the alignment and relaxation dynamics of appended NLO chromophores in poled polymer films is also examined. At temperatures at or above the glass transition temperature, T_g, experimentally measured d_{33} relaxation kinetics of a prototypical chromophore-functionalized polymer, *N*-(4-nitrophenyl)-(*S*)-prolinoxy poly(*p*-hydroxystyrene), (*S*)-NPP-PHS, are well described by the bi-exponential expression predicted by the 3-D model. Below T_g, however, the dynamics are not well modeled as simple 3-D rotational diffusion, the apparent result of complex dynamical matrix interactions. Under all conditions examined, the experimental d_{31} relaxation dynamics can be described approximately using the 2-D model. The temperature dependence of the relaxation rate above T_g is well described by the Williams−Landel−Ferry (WLF) equation, while below T_g, the reorientation process is Arrhenius-like. The d_{33} growth kinetics are found to be accurately approximated using expressions derived from the 3-D rotational diffusion model. Below T_g the experimental activation energy determined from field-on polarization is identical within experimental error to that determined for field-off depolarization.

Introduction

Understanding motion in polymers is a significant problem because of both the technological consequences and the intrinsically challenging physics.[1,2] It is of particular importance in second-order nonlinear optical (NLO) polymers,[3−11] where the kinetics of growth and decay of the second-harmonic signal in response to the initiation or cessation of electric field poling is intimately dependent upon the rotational relaxation rate of the NLO-active chromophore. This relaxation is in turn related to its molecular characteristics and to the nature of the encapsulating polymer matrix. Phenomenological fits to glassy polymer behavior, such as the Kohlrausch−Williams−Watts (KWW) function,[12,13] are useful primarily for correlating material properties and providing information on polymer structure−property relationships.[14] Advancement toward a fuller understanding of such relationships is limited by the lack of appropiate analytical theories and computational models to establish connections between local dynamics and macromolecular structure.

Much attention has been devoted to understanding second-order poled polymers employing molecular-statistical models.[15−21] These are *static models*, however, predicting only steady-state characteristics achieved after *extensive* poling. As a result, if the sample has not been poled for a sufficient time, discrepancies between experiment and theory develop. More importantly, such models provide no insights into the kinetics during or after electric-field poling; these knowledge base parameters are crucial for the design of optimized polymers ultimately suitable for second-order NLO applications.

The goal of the present study is to develop and to evaluate the simplest model for dynamics (isotropic to anisotropic and vice-versa) under electric field poling. This process is modeled using the Smoluchowski diffusion equation, for a dipole in an electric field in both two- and three-dimensional space. The only potential arises from the applied field. The computer-simulated electric field poling/postpoling relaxation profile of the second-harmonic coefficients and their constituent moments can then be accurately evaluated. Both Smoluchowski dynamics[22] and other dynamical approaches based on diffusion[23] have been discussed recently; one aim of this work is to evaluate these diffusion-model results by direct experimental comparison.

Experimentally, we report here time-resolved rotational orientation (*i.e.*, alignment) and reorientation (*i.e.*, post electric field relaxation/decay) studies on the model side-chain chromophore-functionalized polymer system, (*S*)-NPP-PHS, conducted using second-order nonlinear optical (SHG) spectroscopy. These experimental studies are compared to the modeling results permitting evaluation of the dynamic three- and two-dimensional rotational diffusion models as appropriate theoretical frameworks for description of appended chromophore motion in the polymer. Additionally, the results of such analysis are compared to results obtained earlier by employing the empirical KWW function.[24]

Experimental Section

Preparation of Polymer Films. The poly(*p*-hydroxystyrene), PHS, randomly functionalized with the chromophore 4-(4-nitrophenyl)-(*S*)-prolinol ((*S*)-NPPOH), henceforth referred to as (*S*)-NPP-PHS, was synthesized and purified as previously described[14] and was characterized by standard

‡ Current address: Department of Chemistry, Biochemistry, and the Beckman Institute, University of Illinois at Urbana−Champaign.

® Abstract published in *Advance ACS Abstracts,* August 1, 1995.

0024-9297/95/2228-6296$09.00/0

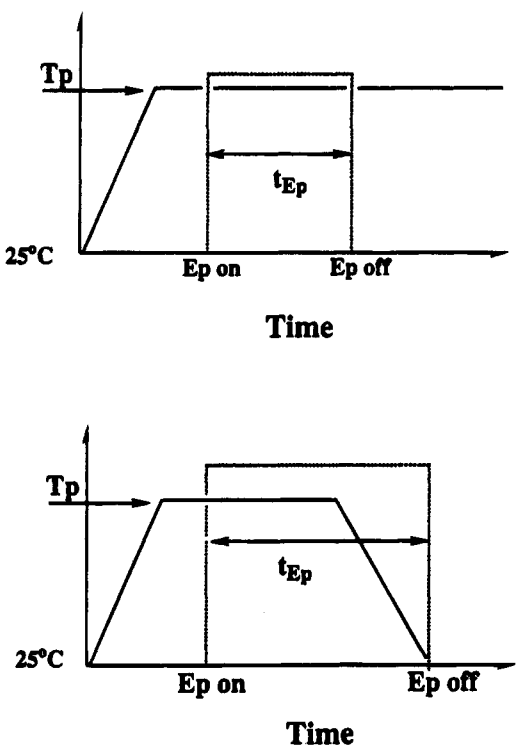

Figure 1. Time–temperature profile for contact (A) and corona (B) poling measurements.

analytical and spectroscopic methodologies. Glass transition temperatures, T_g, defined here as the midpoint of the transition, were measured by differential scanning calorimetry as 146 and 134 °C for 12% and 36% functionalized polymers, respectively (Perkin-Elmer DSC-7, 10 °C/min heating rate). Polymer films were fabricated by dissolution of the polymer powder in freshly distilled THF, followed by multiple filtration through a 0.5 μm syringe filter. The solutions were then cast onto indium tin oxide (ITO)-coated glass substrates in a laminar flow class 100 clean hood. After slow evaporation of solvent at room temperature, the films were heated under vacuum above the glass transition temperature overnight to ensure removal of all traces of solvent and other volatiles that might deleteriously plasticize the polymer matrix. Film thicknesses were determined with an α-Step stylus profilometer (Tencor Instruments).

Contact Poling with in-Situ SHG Monitoring. Thin films of 36% and 12% functionalized (*S*)-NPP-PHS were contact poled with *in-situ* SHG monitoring using the apparatus and configuration previously described.[14] The temperature-dependent transients were collected on annealed (*S*)-NPP-PHS thin films by maintaining the same film temperature, T_p, during both poling (growth) and postpoling (decay) with a constant applied field strength, E_p, and poling time, t_{E_p}. This isothermal timing cycle is presented schematically in Figure 1A. Due to the variety of conditions employed in the experiments discussed herein, the specific poling parameters are provided in the accompanying text. Each sample was irradiated with p-polarized fundamental light (1064 nm), and the p-polarized second-harmonic light generated from the samples was measured. The second-harmonic intensity (532 nm) was recorded using the p–p configuration (I_{pp}).

Corona Poling with in-Situ SHG Monitoring. The annealed (*S*)-NPP-PHS thin films were corona poled *in-situ*, using the apparatus and configuration previously described.[14] The samples were nonisothermally poled, *i.e.*, poled at elevated temperatures with decay measurements made at room temperature, using the timing sequence illustrated in Figure 1B. This procedure involves heating the polymer film to the selected temperature, T_p, and after thermal equilibrium is established, applying the corona voltage (+5.0 kV). Upon completion of poling (t_{E_p} = 30 min), the film samples are cooled to room temperature at a rate of ca. 10 °C/min in the presence of the field. SHG data are taken after 30 min of room temperature storage. SHG measurements were conducted at 1064 nm in both the p–p and s–p polarized geometries. Each sample was irradiated with linearly p-polarized fundamental light (1064 nm) and the p-polarized second harmonic light (532 nm) generated from the samples measured.

Data Analysis. Linear and nonlinear least-squares analysis of the various SHG signal components was performed using a commercially available software package (Kaleidagraph, Version 2.1, Synergy Software, Reading, PA). The best model is defined as that meeting the following criteria: (1) the simplest model (*i.e.*, having the minimum number of adjustable parametrs), (2) smallest residual/goodness of fit, and (3) smallest uncertainties in the fit parameters as determined by nonlinear least-square analysis.

Theory

Static Description of Electric Field Poling. SHG is a sensitive probe of molecular orientation. Therefore, by examination and analysis of the bulk NLO response of a poled chromophore-functionalized polymer, information can be obtained on the orientational distribution of the NLO-active chromophore units. In samples where a polar axis (*i.e.*, imposed $C_{\infty v}$ symmetry) has been induced (poled polymers), the relationship between macroscopic and microscopic second-harmonic properties for quasi-one-dimensional molecules (*i.e.*, in which the dipole moment is directed along the symmetry axis such that the β_{zzz} component dominates) is given by only two independent nonvanishing components of $\chi^{(2)}_{ijk}$.[25] This is in contrast to the general case where there are 18 relevant second-order NLO coefficients.

$$\chi^{(2)}_{zzz} = N\beta_{zzz} f^{2\omega} f^{\omega} f^{\omega} \langle \cos^3 \theta \rangle \quad (1)$$

$$\chi^{(2)}_{zxx} = \chi^{(2)}_{zyy} = \frac{1}{2} N\beta_{zzz} f^{2\omega} f^{\omega} f^{\omega} \langle \cos \theta \sin^2 \theta \rangle = \frac{1}{2} N\beta_{zzz} f^{2\omega} f^{\omega} f^{\omega} [\langle \cos \theta \rangle - \langle \cos^3 \theta \rangle] \quad (2)$$

In the above equations, $\chi^{(2)}_{zxx}$, $\chi^{(2)}_{zyy}$, and $\chi^{(2)}_{zzz}$ are the macroscopic second-order susceptibility tensors, N is the chromophore number density, β_{zzz} is a component of the molecular hyperpolarizability tensor, β, and $\langle \cos \theta \rangle$ and $\langle \cos^3 \theta \rangle$ are angular averages which describe the degree of polar order achieved during poling. Thus, to model second-harmonic generation in poled polymers, the first and third moments, $\langle \cos \theta \rangle$ and $\langle \cos^3 \theta \rangle$, must be evaluated. A static theoretical description of dipolar alignment in the presence of an electric field can be used to calculate these orientational order parameters at equilibrium. A variety of statistical–mechanical descriptions have been published.[15-20] Four of these, the isotropic model,[15,16] the Ising model,[15,16] the SKS (Singer–Kuzyk–Sohn) model,[17] and the MSVP (Maier–Saupe–Van der Vorst–Pickens) model[18,19] consider only isolated dipoles. The major difference among them is the choice of single particle potential. Recently, Wang has proposed another statistical–mechanical model which includes the effect of pair orientational correlation.[20,21]

The molecular-statistical model describes the interaction of an isolated, uniaxial molecule with its environment. The permanent dipole, μ, is at an angle, θ, with respect to the field, and its energy in the field is given by

$$V(\theta) = -\mu E \cos \theta \quad (3)$$

Using the Boltzmann distribution, the net moment is given as

$$\langle z(\theta)\rangle_{eq} = \frac{\int_0^\pi e^{(u\cos\theta)} z(\theta)\sin\theta\, d\theta}{\int_0^\pi e^{(u\cos\theta)}\sin\theta\, d\theta} \quad (4)$$

Here $u = \mu E/kT$, k is the Boltzmann constant, T is the thermodynamic temperature, μ is the dipole moment of the uniaxial molecule, E is the strength of the applied field, θ is the spherical polar angle between the molecular dipole axis and the direction of the field (Figure 2), and $z(\theta)$ is either $\cos\theta$ or $\cos^3\theta$.

Evaluating the integrals in eq 4 analytically and considering the limit of small dipolar alignment ($E < 1$ MV/cm) permit the determination of a ratio of the macroscopic second-harmonic susceptibility tensors (eq 5). (Note these are generally referred to as "d coefficients", with d_{33} and d_{31} representing $^1/_2\chi^{(2)}_{zzz}$ and $^1/_2\chi^{(2)}_{zxx}$, respectively). This model provides

$$R = \frac{\chi^{(2)}_{zzz}}{\chi^{(2)}_{zxx}} = \frac{d_{33}}{d_{31}} = \frac{\langle\cos^3\theta\rangle}{\frac{1}{2}(\langle\cos\theta\rangle - \langle\cos^3\theta\rangle)} \approx 3.00 \quad (5)$$

valuable information on the polar parameters and, ultimately, on the bulk second-order NLO properties corresponding to the thermodynamically stable configuration. This approach, however, provides no information on what occurs *during* the approach to steady state or subsequent to cessation of poling. We address these limitations by developing and evaluating the simplest diffusion models for the time evolution of the poling and postpoling processes. We examine their appropriateness for the description of appended chromophore motion during and after electric field poling, as experimentally measured by SHG. The diffusivities obtained upon analysis of the experimental rise and decay transients are then used to evaluate the kinetics and thermodynamics of dipolar relaxation. Comparisons are made to the results obtained by previous studies employing the empirical KWW function.[24]

Dynamic Rotational Diffusion. Brownian motion,[26,27] the continuous changes in both polymer shape and position induced by thermal agitation, is the *simplest* way to picture time-dependent phenomena in polymers, including diffusion. The present work details the application of the Smoluchowski diffusion equation (the strongly damped Fokker–Planck equation in coordinate space) to describe the temporal behavior of an NLO-active dipole immersed in a viscous matrix (amorphous polymer) during and after electric field poling. Specifically, the rotational motion of rodlike molecules in the presence or absence of a static external electric field is examined. Examination of the rise and decay transients for a given system permits exclusion of alignment and relaxation mechanisms inconsistent with the data and provides information on the actual molecular mechanism. The present pragmatic model is admittedly oversimplified, since actual relaxation processes in polymers occur on many time scales;[1,12,13,28–34] complex memory-kernel approaches,[32] rather than the simple damping with a single, constant rotational diffusion coefficient as employed here, are a more appropriate framework to describe relaxation and transport in such systems. Our aim here is to apply and test the simplest rotational diffusion model, to compare both its successes and its failures with observed poling dynamics.

Dynamic Two-Dimensional Rotational Diffusion. The rotational diffusion of a rigid rotor in a plane

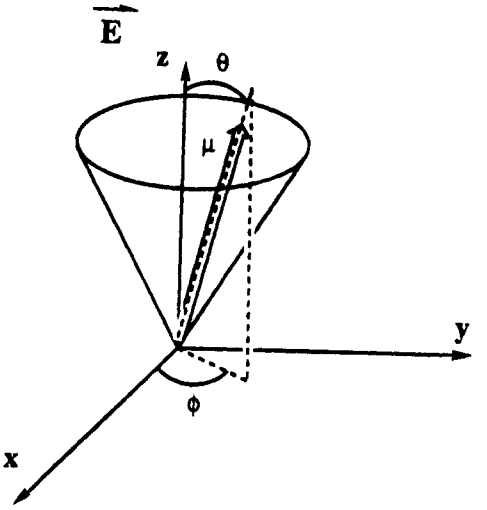

Figure 2. Three-dimensional rotational diffusion model of a polar molecule in the presence of an external field. θ is the spherical polar angle between the principal molecular dipole axis, μ, and the field, E. ϕ is the azimuthal angle.

containing the external electric field is described by the 2-D Smoluchowski equation[28] where D_R is the rotational diffusion coefficient. This equation gives the time evolution of the

$$\frac{\partial f(\theta,t)}{\partial t} = D_R\frac{\partial}{\partial\theta}\left[\frac{\partial f(\theta,t)}{\partial\theta} + \frac{\partial V(\theta)}{\partial\theta}\frac{f}{kT}\right] \quad (6)$$

probability, $f(\theta,t)$, that the molecular axis is pointing in the direction θ. The interaction Hamiltonian, $V(\theta)$, of the molecule with the applied field depends upon the polar angle between the molecular axis and the field (Figure 2), and is given by eq 3. Appendix A presents the detailed solution.

A ratio of the second-order NLO or d coefficients, R, of 6.00 is predicted for the 2-D model in the low-field limit by substituting eqs A6 and A7 into eq 5,

$$R = \frac{\langle\cos^3\theta\rangle}{\frac{1}{2}[\langle\cos\theta\rangle - \langle\cos^3\theta\rangle]} \approx \frac{\frac{3}{8}\left(\frac{f_{-1}+f_1}{f_0}\right)}{\frac{1}{2}\left[\frac{1}{2}\left(\frac{f_{-1}+f_1}{f_0}\right) - \frac{3}{8}\left(\frac{f_{-1}+f_1}{f_0}\right)\right]} \approx 6.00 \quad (7)$$

This value has been observed experimentally for chromophore molecules bound to certain linear polymers.[36] In these systems, having chromophore-functionalized linear polymers with small spacer units, it has been proposed that movements of the tethered dipoles are constrained to two dimensions, that is, to a plane perpendicular to the polymer backbone. In actuality, however, many systems do not behave in a perfectly 2-D manner, but rather incorporate some degree of 3-D character. Therefore, experimentally, one would expect to observe a range of R values between 3.0 (completely isotropic as predicted by the 3-D static model) and 6.0 (completely 2-D), depending upon the system. A full range of R values has been reported in the literature; however, the majority are close to $R = 3.0$.[37–43] A fuller discussion will be presented in a forthcoming contribution.[44]

Once the poling phase of the cycle has been completed, the second-harmonic coefficients decay as the molecules

rotationally diffuse toward an isotropic distribution. The 2-D diffusion equation then becomes

$$\frac{\partial f(\theta,t)}{\partial t} = D\frac{\partial^2 f(\theta,t)}{\partial \theta^2} \tag{8}$$

Using the same analysis described in Appendix A for the field-on case, we find

$$\frac{\mathrm{d}f_{m'}(t)}{\mathrm{d}t} = -D_R m'^2 f_{m'}(t) \tag{9}$$

Thus, field-free decay or simple rotational diffusion is described by first-order kinetics. Solving this differential equation yields

$$f_{m'}(t) = f_{m'}(0)\, \mathrm{e}^{-D_R m'^2 t} \tag{10}$$

This integrated rate law describes the decay process as multiple exponential, with each term in the expansion having a characteristic relaxation constant, $k_r = D_R m'^2$. Thus, the decay of the second-order NLO coefficients is effectively governed by the rotational diffusion coefficient, D_R. Substitution of the appropriate $f_{m'}(t)$'s, from eq 10 into eq A7 yields the following relationship describing the time-dependent dynamics of the third moment of θ ($\propto d_{33}$)

$$\frac{\langle\cos^3\theta\rangle(t)}{\langle\cos^3\theta\rangle(0)} = \frac{f_{-1}(0)+f_1(0)}{f_{-3}(0)+3f_{-1}(0)+f_3(0)+3f_1(0)}\mathrm{e}^{-D_R t} + \frac{f_3(0)+f_{-3}(0)}{f_{-3}(0)+3f_{-1}(0)+f_3(0)+3f_1(0)}\mathrm{e}^{-9D_R t} \tag{11}$$

All variables retain their usual meaning, and the f_m coefficients at $t = 0$ are those found immediately prior to field removal. Here, the first component of the relaxation dynamics is characterized by the third-order Legendre polynomial possessing an average relaxation time, $\tau_{P3} = (9D_R)^{-1}$. The slow relaxation component is characterized by the first-order Legendre polynomial with a relaxation time $\tau_{P1} = (D_R)^{-1}$. Equation 11 can be further simplified by re-expressing the pre-exponential coefficients as W_1 and W_3, respectively, resulting in a generalized form describing the postpoling relaxation dynamics in two-dimensional space.

$$\sqrt{\frac{I(t)_{pp}}{I(0)_{pp}}} = W_1\mathrm{e}^{-D_R t} + W_3\mathrm{e}^{-9D_R t} \tag{12}$$

In a fashion similar to that described above, an equation describing the field-free relaxation dynamics of the d_{31} second-harmonic coefficient in 2-D space may be derived. In two dimensions, d_{31} is related to the probability coefficients according to the following equation:

$$d_{31} = \frac{1}{2}[\langle\cos\theta\rangle - \langle\cos^3\theta\rangle] = \left[\frac{f_1+f_{-1}}{2f_0} - \frac{f_{-3}+3f_{-1}+3f_1+f_3}{8f_0}\right] \tag{13}$$

With substitution of the required $f_{m'}(t)$'s according to eq 10 and recognition that the $f_{m'}(t)$ values are symmetric about $f_0(t)$ (*i.e.*, $f_1 = f_{-1}$ and $f_3 = f_{-3}$), eq 13 yields the following function describing the time-dependent, postpoling dynamics of the d_{31} second-harmonic coefficient:

$$\sqrt{\frac{I(t)_{sp}}{I(0)_{sp}}} = \frac{d(t)_{31}}{d(0)_{31}} = \frac{f_1(0)}{f_1(0)-f_3(0)}\mathrm{e}^{-D_R t} + \frac{-f_3(0)}{f_1(0)-f_3(0)}\mathrm{e}^{-9D_R t} \tag{14}$$

For nonlinear least-squares fitting, eq 14 can be simplified by re-expression of the pre-exponential coefficients as $\hat{W}_1$ and $\hat{W}_3$, respectively, resulting in a generalized bi-exponential function identical to that derived for d_{33} decay confined to two-dimensions (eq 12),

$$\sqrt{\frac{I(t)_{sp}}{I(0)_{sp}}} = \hat{W}_1\mathrm{e}^{-D_R t} + \hat{W}_3\mathrm{e}^{-9D_R t} \tag{15}$$

Dynamic Three-Dimensional Rotational Diffusion. In three dimensions in the presence of an electric field (*i.e.*, an axially symmetric system, Figure 2), the rotational diffusion of a rigid rod is described by[45]

$$\frac{1}{D_R}\frac{\partial f(\theta,t)}{\partial t} = \frac{1}{\sin\theta}\frac{\partial}{\partial\theta}\left\{\sin\theta\left[\frac{\partial f(\theta,t)}{\partial\theta} + \frac{f(\theta,t)}{kT}\frac{\partial V}{\partial\theta}\right]\right\} \tag{16}$$

Here, $f(\theta,t)$ is the probability of obtaining the dipole vector in an orientation θ at time t. The hydrodynamic parameter of interest is D_R, the rotational diffusion coefficient. The potential energy, $V(\theta)$, is again described by eq 3. As shown in Appendix B an analytic solution to the rotational diffusion equation can be found by expansion in orthogonal functions.

A ratio of the second-harmonic coefficients, R, of 3.00 is predicted for the low-field, three-dimensional model by substituting eqs B7 and B8 into eq 5,

$$R = \frac{\langle\cos^3\theta\rangle}{\frac{1}{2}[\langle\cos\theta\rangle - \langle\cos^3\theta\rangle]} \approx \frac{\frac{f_1}{5f_0}}{\frac{1}{2}\left[\frac{f_1}{3f_0} - \frac{f_1}{5f_0}\right]} \approx 3.00 \tag{17}$$

Upon sudden removal of the electric field, the dipolar chromophores disorient by Brownian motion, and the second-order NLO signal decays. Since the chromophores are released from the aligned state (*i.e.*, the orienting field), the diffusion equation reduces to

$$\frac{\mathrm{d}f_{m'}}{\mathrm{d}t} = -D_R m'(m'+1)f_{m'} \tag{18}$$

Integration yields

$$f_{m'}(t) = f_{m'}(0)\, \mathrm{e}^{-D_R m'(m'+1)t} \tag{19}$$

where $f_{m'}(0)$ is the initial value of the probabilities. The integrated rate law describes the decay process for each m' as a simple exponential, with each Legendre polynomial possessing a characteristic relaxation constant, k_r, equal to $D_R m'(m'+1)$. Substitution of the required time-dependent probabilities into eqs B10 and B11 yields an expression for the $\langle\cos^3\theta\rangle$ ($\propto d_{33}$) depolarization dynamics.

$$\frac{\langle\cos^3\theta\rangle(t)}{\langle\cos^3\theta\rangle(0)} = \frac{7f_1(0)}{2f_3(0)+7f_1(0)}e^{-2D_R t} + \frac{2f_3(0)}{2f_3(0)+7f_1(0)}e^{-12D_R t} \quad (20)$$

The f_m values at $t = 0$ are those found immediately prior to field termination, since the above equation describes only the post electric field relaxation. Equation 20 indicates that the fast component of the chromophore relaxation dynamics is characterized by the third-order Legendre polynomial, $P_3(\cos\theta)$, with an average relaxation time of $\tau_{P_3} = (12D_R)^{-1}$, while the slower component is characterized by the first-order Legendre polynomial, $P_1(\cos\theta)$, with a relaxation time of $\tau_{P_1} = (2D_R)^{-1}$. The form of eq 20 resembles the empirical bi-exponential function frequently discussed in studies of NLO polymer dynamics,[4-11] and eq 20 thus provides some theoretical justification for fitting the chromophore randomization process after electric-field removal to a sum of exponentials.

Recasting the pre-exponential coefficients in eq 20 as

$$W'_1 = \frac{7f_1(0)}{2f_3(0)+7f_1(0)} \quad (21)$$

and

$$W'_3 = \frac{2f_3(0)}{2f_3(0)+7f_1(0)} \quad (22)$$

we find, for the 3-D rotational diffusion,

$$\sqrt{\frac{I(t)_{pp}}{I(0)_{pp}}} = W'_1 e^{-2D_R t} + W'_3 e^{-12D_R t} \quad (23)$$

with W'_1 and W'_3 contributions to the total decay from the fast and slow components.

Analysis of the Field-Free $\langle\cos\theta\rangle$ Decay. It follows from eqs B11 and 19 that

$$\frac{\langle\cos\theta\rangle(t)}{\langle\cos\theta\rangle(0)} = e^{-2D_R t} \quad (24)$$

This equation predicts that the decay of $\langle\cos\theta\rangle$ will be a single exponential characteristic of the first-order Legendre polynomial, with a relaxation time $\tau_1 = (2D_R)^{-1}$.

Analysis of the Field-Free Decay of d_{31}. From eqs B8 and B11 we see that

$$d_{31} = \frac{1}{2}[\langle\cos\theta\rangle - \langle\cos^3\theta\rangle] = \left[\frac{f_1}{15f_0} - \frac{f_3}{35f_0}\right] \quad (25)$$

Then from eqs 19 and 25,

$$\sqrt{\frac{I(t)_{sp}}{I(0)_{sp}}} = \frac{d(t)_{31}}{d(0)_{31}} = \frac{7f_1(0)}{7f_1(0)-3f_3(0)}e^{-2D_R t} + \frac{-3f_3(0)}{7f_1(0)-3f_3(0)}e^{-12D_R t} \quad (26)$$

In the above equation, the $f_m(0)$ values are those found immediately prior to field termination. Renaming of the pre-exponential coefficients as

$$W''_1 = \frac{7f_1(0)}{7f_1(0)-3f_3(0)} \quad (27)$$

and

$$W''_3 = \frac{-3f_3(0)}{7f_1(0)-3f_3(0)} \quad (28)$$

then gives

$$\sqrt{\frac{I(t)_{sp}}{I(0)_{sp}}} = W''_1 e^{-2D_R t} + W''_3 e^{-12D_R t} \quad (29)$$

The pre-exponential coefficients W''_1 and W''_3 can be viewed as the fractional contributions of the fast and slow components of the total decay; eq 29 is identical in *form* to that derived previously for d_{33} relaxation (eq 23). The specific differences between field-free d_{33} and d_{31} dynamics reside solely in the explicit form of the pre-exponential coefficients.

Analysis of the Field-on Growth of $\langle\cos^3\theta\rangle$. As detailed in a preceding section, eq B7 provides an analytic solution to the 3-D rotational diffusion equation of a dipole in the presence of an external electric field. Unlike the field-off case, this recursion formula couples the probability coefficient, $f_{m'}(t)$, to both $f_{m+1'}(t)$ and $f_{m'-1}(t)$. Therefore, the equation cannot be straightforwardly integrated. Solutions may be obtained, however, by assuming a specific $\mu E/kT$ ratio (which will be defined as a dimensionless poling parameter, u) and solving

$$\dot{\overline{f(t)}} = \overline{T}\overline{\lambda}\overline{T^{-1}}\overline{f(0)} \quad (30)$$

In this equation, $\dot{\overline{f(t)}}$ is a vector of the probability coefficients of interest, $\overline{T}$ is a matrix of eigenvectors, $\overline{\lambda}$ is a diagonal matrix of eigenvalues, and $\overline{f(0)}$ is the initial value matrix ($f_m(0) = {}^1/_2\delta_{mj}$, with δ_{ij} the Kroneker delta). Multiplying the matrices on the right side of eq 30 results in the following general expressions for the f_0, f_1, and f_3 probability coefficients:

$$f_0(t) = W_{00}e^{\lambda_0 D_R t} + W_{01}e^{\lambda_1 D_R t} + W_{02}e^{\lambda_2 D_R t} + W_{03}e^{\lambda_3 D_R t} \quad (31)$$

$$f_1(t) = W_{10}e^{\lambda_0 D_R t} + W_{11}e^{\lambda_1 D_R t} + W_{12}e^{\lambda_2 D_R t} + W_{13}e^{\lambda_3 D_R t} \quad (32)$$

$$f_3(t) = W_{30}e^{\lambda_0 D_R t} + W_{31}e^{\lambda_1 D_R t} + W_{32}e^{\lambda_2 D_R t} + W_{33}e^{\lambda_3 D_R t} \quad (33)$$

In these expressions, λ_m is the mth eigenvalue. The particular solutions will depend on the u parameter determining the degree of coupling between Legendre polynomials.

We consider first the case of a small poling parameter, $u = 0.1$. Here $f_3(t)$ makes a negligible contribution relative to $f_1(t)$ and $f_0(t)$. In addition, all terms greater than the second exponential term in the expression for $f_1(t)$ and all terms greater than the first exponential in the expression for $f_0(t)$ may be neglected. These approximations simplify to

$$f_0(t) = W_{00}e^{0.033 D_R t} \quad (34)$$

$$f_1(t) = W_{10}e^{0.033 D_R t} - W_{11}e^{-2.01 D_R t} \quad (35)$$

Substitution of these expressions into eq B10 yields the following general relationship describing the growth of the second-harmonic signal ($\langle\cos^3\theta\rangle$), at small u (0.1):

$$\frac{\langle\cos^3\theta\rangle(t)}{\langle\cos^3\theta\rangle(0)} = \frac{W_{10}}{W_{10}-W_{11}} - \frac{W_{11}}{W_{10}-W_{11}}e^{-2.04D_R t} \quad (36)$$

Renaming the ratios of constants, $W_{11}/(W_{10}-W_{11})$ and $W_{10}/(W_{10}-W_{11})$ as W_1 and N, respectively, results in an expression suitable for nonlinear least-squares analysis,

$$\frac{\langle\cos^3\theta\rangle(t)}{\langle\cos^3\theta\rangle(0)} = N - W_1 e^{-2.04D_R t} \quad (37)$$

so at small u, the chromophore alignment dynamics are predicted to be exponential.

If the u parameter is increased to 0.5, neglecting all terms for which the pre-exponential coefficients are less than 10^{-1} followed by generalization of the remaining pre-exponential coefficients gives

$$f_0(t) = W_{00}e^{0.7D_R t} + W_{01}e^{-2.2D_R t} \quad (38)$$

$$f_1(t) = W_{10}e^{0.7D_R t} + W_{11}e^{-2.2D_R t} \quad (39)$$

Thus, for $u = 0.5$,

$$\frac{\langle\cos^3\theta\rangle(t)}{\langle\cos^3\theta\rangle(0)} = N\left(\frac{1-(W_1+W_2)e^{-2.9D_R t}}{1+W_1 e^{-2.9D_R t}}\right) \quad (40)$$

Although increasing u causes the SHG rise function to change in form, the behavior is still dominated by a single exponential.

In the limit of a large poling parameter (*i.e.*, large fields), we have

$$f_0(t) = W_{00}e^{2.2D_R t} + W_{01}e^{-2.2D_R t}$$

$$f_1(t) = W_{10}e^{2.2D_R t} - W_{11}e^{-2.2D_R t}$$

$$f_3(t) = -W_{31}e^{-2.2D_R t} + W_{32}e^{-6.5D_R t}$$

For an increased poling parameter, a larger number of exponential terms must be included to accurately characterize the growth of the SHG signal, implying greater coupling or mixing of the higher order Legendre polynomials. This is consistent with previous results which showed that increasing field strength increased the distribution of relaxation times (*i.e.*, decrease in the KWW β parameter for the fitting function applied to the SHG signal transients).[24]

Results and Discussion

We evaluate herein the appropriateness of the two- and three-dimensional rotational diffusion models derived above for describing appended chromophore motion during and after electric field poling. The results are interpreted using free volume arguments. Furthermore, the diffusivities obtained upon analysis of the experimental decay and rise transients are used to evaluate the kinetics and thermodynamics of dipolar relaxation. Comparisons are made to the results obtained by previous studies employing the empirical KWW function.[24,50-52]

The diffusion process governing the time-dependent second-harmonic intensity ($\sqrt{I_{pp}} \propto d_{33}$) following removal of the external field (*i.e.*, relaxation dynamics) can be analyzed by applying the first-order kinetic description from the 3-D rotational diffusion model. The rise and decay transients of the second-harmonic d coefficients, d_{31} and d_{33}, as revealed through their constituent moments, $\langle\cos\theta\rangle$ and $\langle\cos^3\theta\rangle$, for $u = (\mu E/kT) = 0.1$ are plotted in Figure 3. In this plot, the assumed rotational diffusion coefficient ($D_R = 1.5 \times 10^{-5}$ rad^2/s) is the same for both signal growth and decay. (Nearly identical diffusivities would correspond to isothermal poling, without aging above T_g). The maximum values of the moments of cos θ at steady state ($\langle\cos^3\theta\rangle = 0.40 \times 10^{-1}$, $\frac{1}{2}[\langle\cos\theta\rangle - \langle\cos^3\theta\rangle] = 0.13 \times 10^{-1}$) correspond exactly to those values predicted using the simple, static statistical model. Comparison of the transients generated by the 3-D model to those using the 2-D model (Figure 4) show that the correlation times for both the rise and decay curves in the 2-D model are significantly longer (Figure 4). Although $\langle\cos^3\theta\rangle$ ($\propto d_{33}$) approaches the asymptote at a lower rate, the same plateau value is eventually attained. In contrast, the steady-state value of the first moment is substantially lower in the 2-D model than in the 3-D model.

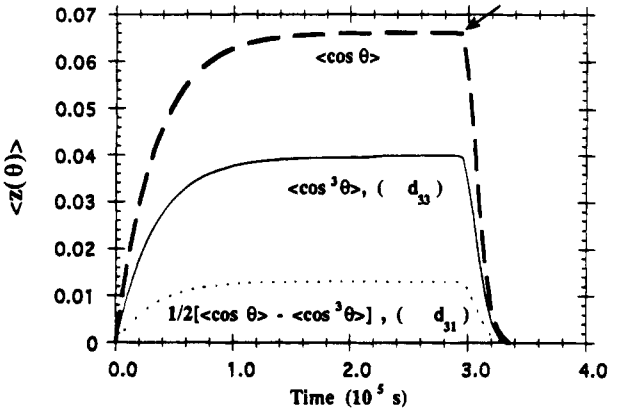

Figure 3. Theoretical growth and decay transients of the pertinent dynamical quantities $\langle\cos\theta\rangle$ and $\langle\cos^3\theta\rangle$ based upon the three-dimensional rotation diffusion model. Simulation parameters: $\mu = 2.34 \times 10^{-29}$ C m, $E = 2.50 \times 10^7$ V/m, $T = 423$ K, D_R(on) = D_R(off) = 1.45×10^{-5} rad^2/s. The arrow indicates time of field termination.

As shown in Figure 5, the characteristic time with which the dynamical quantities approach the asymptotic values and the maximum values are achieved depends strongly on the magnitude of the poling field strength (*i.e.*, u). Figure 6 shows that the third moment saturates at high fields, $u > 20$ (10 MV/cm) with deviations from linearity observed at approximately 1.3 MV/cm. This theoretical prediction of deviation from linearity at high field strengths, agrees well with previous experimental findings.[14] Theoretical predictions of the pre-exponential coefficients, W'_1 and W'_3, can readily be examined under various simulation conditions by explicit determination of the f_m values and applying eqs 21 and 22. The results, summarized in Table 1, indicate that W'_1, hence the probability coefficient f_1, is dominant, with only minor contributions arising from W'_3 (*i.e.*, f_3). Changes in simulation parameters such as temperature and field strength are only minor perturbations on the relative contributions, although a slightly more pronounced increase in the W'_3 contribution is found with increasing field strength.

Analysis of Experimental Field-Free Decay of $\langle\cos^3\theta\rangle$. To examine experimentally the validity of the general functional form predicted by the 3-D diffusion model, a series of isothermal SHG relaxation transients (*i.e.*, decay transients for which the same temperature

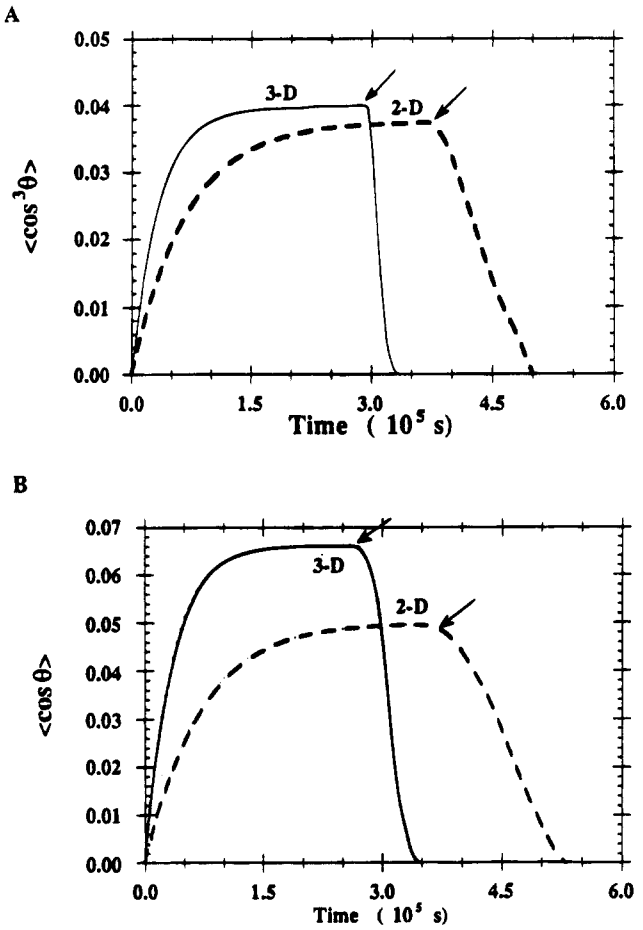

Figure 4. Comparison of the time-dependent behavior of the $\langle\cos^3\theta\rangle$ and $\langle\cos\theta\rangle$ orientational order parameters as calculated using the 2-D and 3-D rotational diffusion models. Simulation parameters: $\mu = 2.34 \times 10^{-29}$ C m, $E = 2.50 \times 10^7$ V/m, $T = 423$ K, $D_R(\text{on}) = D_R(\text{off}) = 1.45 \times 10^{-5}$ rad²/s. The arrows indicate time of poling field termination.

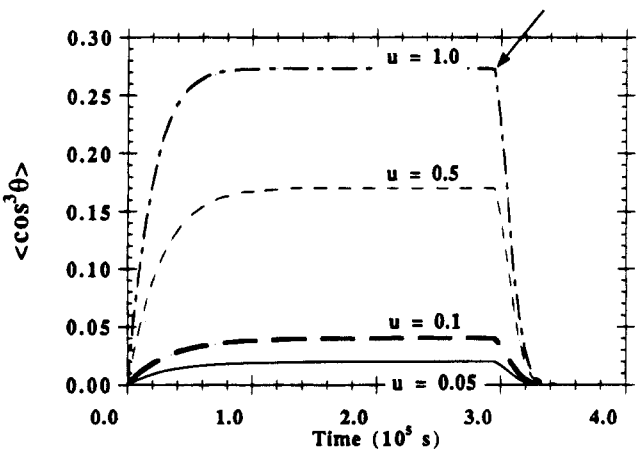

Figure 5. Dependence of transient behavior of $\langle\cos^3\theta\rangle$ on electric poling field strength. For all runs: $\mu = 2.34 \times 10^{-29}$ C m, $T = 423$ K, $D_R(\text{on}) = D_R(\text{off}) = 1.45 \times 10^{-5}$ rad²/s. For $u = 0.05$, $E = 1.25 \times 10^7$ V/m; $u = 0.1$ ($u = \mu E/kT$), $E = 2.50 \times 10^7$ V/m; $u = 0.5$, $E = 1.25 \times 10^8$ V/m; $u = 1.0$, $E = 2.50 \times 10^8$ V/m. The arrow indicates time of poling field termination.

is maintained both during and after poling) for a poled, functionalized NLO polymer (Figure 7) were fit to eq 23. Table 2 shows that W_3 (which describes the magnitude of the fast component) approaches unity at poling temperatures well above T_g. The temperature dependence of W_1 and W_3 is illustrated in Figure 8. The transient behavior behavior at 153 °C (20 deg above T_g) of 36% functionalized (*S*)-NPP-PHS indicates that the

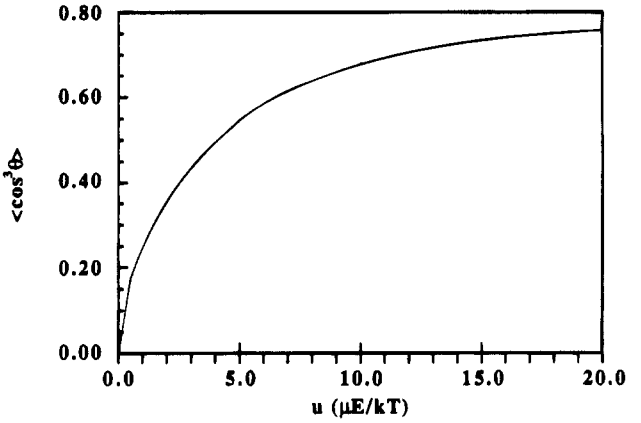

Figure 6. Field-dependent behavior of $\langle\cos^3\theta\rangle$. Simulation parameters: $\mu = 2.34 \times 10^{-29}$ C m, $T = 423$ K, $D_R(\text{on}) = D_R(\text{off}) = 1.45 \times 10^{-5}$ rad²/s.

Table 1. Theoretically Predicted Changes in the Pre-Exponential Coefficients of Eq 23 As Determined by Computer-Modeled Electric Field Poling Using the Three-Dimensional Rotational Diffusion Model

temp (°C)	poling field strength, E (V/m)	diffusion coeff, D_R (rad²/s)	W'_1[a]	W'_3[a]
130	2.5×10^7	1.5×10^{-5}	1.00	1.57×10^{-5}
50	2.5×10^7	1.5×10^{-5}	0.999	1.29×10^{-3}
130	2.5×10^8	1.5×10^{-5}	0.945	0.0550
50	2.5×10^8	1.5×10^{-5}	0.929	0.0712

[a] Coefficients calculated by insertion of appropriate probability coefficients into eqs 21 and 22. The $f_1(0)$ and $f_3(0)$ values used were those theoretically determined immediately prior to field cessation.

relaxation dynamics are nearly completely dominated by single exponential decay. The general experimental form agrees well with theoretical predictions (Table 1). Our simple 3-D Smoluchowski theory, however, predicts that the relaxation dynamics should be single exponential, characteristic of $P_1(\cos\theta)$, whereas experimentally we apparently find it characteristic of $P_3(\cos\theta)$. The fits are, however, not definitive in the region in which either W'_1 or W'_3 exceeds 0.9. In this range, a single term dominates. Figure 7B plots the same data shown in Figure 7A semilogarithmically. It is clear, as the numbers in Table 2 suggest, that at the highest temperatures, a single exponential fits the data rather well; in the absence of information on the diffusion coefficients, it is then impossible to say simply from curve fitting, whether W_1 or W_3 is dominant in this regime. Thus, in the nearly single exponential regime, distinctions between f_3 and f_1 behavior cannot be clearly drawn from SHG relaxation dynamics alone.

The relaxation transients collected between 153 °C and T_g are best fit by a bi-exponential function with a dominant W_3 contribution (Table 2). The diminished contribution from W_1 may arise from the fact that at temperatures sufficiently far above T_g (*i.e.*, in the rubbery state), the polymer is sufficiently fluid to allow the fast relaxation processes to dominate. As the temperature decreases, however, contributions from the slow rate processes become increasingly significant until, at 20 deg below T_g, the W_1 contribution dominates. Thus, decreasing temperature leads to progressive hindrance of chromophore rotation, which can be interpreted as a reduction in free volume to below the critical size required for unimpeded chromophore reorientation.

At temperatures at and below T_g (115–134 °C), the transient dynamics become substantially more complex. The results of least-squares analysis (Table 2) show not only significant contributions from both Legendre poly-

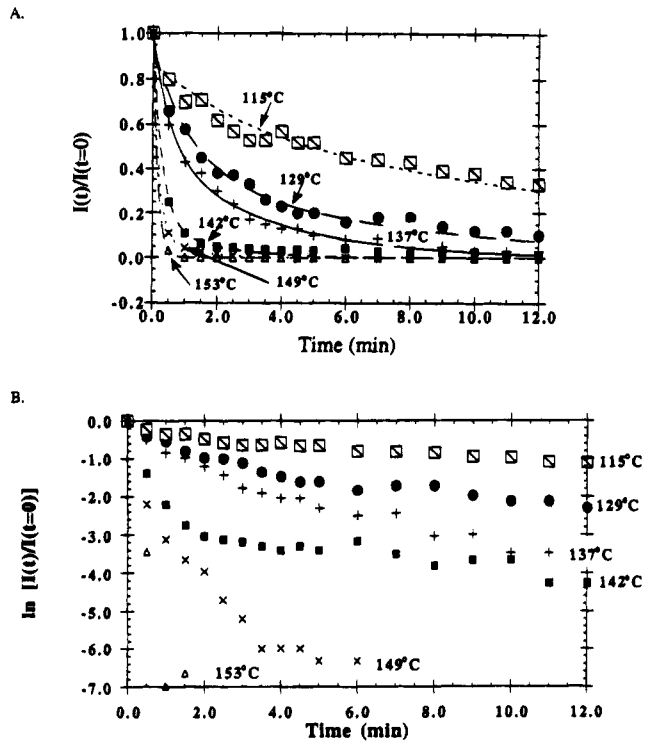

Figure 7. (A) Experimental SHG decay transients collected at various temperatures above and below T_g, for contact-poled (E_p = 1.1 MV/cm; t_{E_p} = 16 min) 36% functionalized (*S*)-NPP-PHS films. Lines are nonlinear least-squares fits to eq 23. Error bars for data points are equal to or less than the symbol dimensions. The 134 °C data have been omitted for ease of viewing. (B) Semilogarithmic plot of the data of Figure 7A.

Table 2. Summary of Nonlinear Least-Squares Fitting of Data Presented in Figure 7 to Eq 23[a]

temp (°C)	W_3	W_1	D_R (rad²/min)	goodness of fit
115	0.29(0.44)	0.59(0.44)	0.028(0.031)	0.961
129	0.55(0.10)	0.34(0.11)	0.059(0.003)	0.990
134	0.52(0.16)	0.43(0.20)	0.14(0.01)	0.981
137	0.65(0.08)	0.33(0.08)	0.16(0.01)	0.995
142	0.84(0.06)	0.16(0.06)	0.29(0.02)	0.996
149	0.88(0.01)	0.12(0.01)	0.52(0.02)	0.999
153	0.998(0.001)	0.0016(0.001)	0.58(0.003)	0.999

[a] Numbers in parentheses are standard deviations.

nomials, $P_1(\cos\theta)$ and $P_3(\cos\theta)$, but also that the weighting coefficients, W_1 and W_3, do not sum to unity as expected. (The SHG intensity was normalized to unity at $t = 0$, and therefore, the sum of the weighting coefficients should equal unity). This may indicate that a bi-exponential function (eq 23) is not appropriate and that additional exponential terms are required to adequately describe the glassy state relaxation dynamics. A further indication of the inadequacy of the bi-exponential form at lower temperatures is found both in visual inspection of the fits and in the fit statistics (*i.e.*, uncertainties in the fit parameters and the residual/goodness of fit parameter). These observations clearly indicate a breakdown of the simple rotational diffusion models.

The Kohlrausch–Williams–Watts (KWW) equation is an empirical function which has been applied to evaluate the SHG decay in a variety of NLO polymer systems.[24,50,51] The KWW function (eq 41)

$$\phi(t) = e^{-(t/\tau)^{\beta}} \tag{41}$$

describes relaxation behavior as a distribution of relaxation processes where $\phi(t)$ represents the normalized relaxation function, τ is the average or most probable relaxation time, and β is a constant between 0 and 1 which indicates the breadth of distribution of τ's. For poled (*S*)-NPP-PHS films, we find that the dispersion index β increases with increasing temperature, indicating that the distribution of relaxation times sharpens with increasing temperature.[24,50–52] This parallels the above findings employing the rotational diffusion models, *i.e.*, monoexponential decay characterized by a single relaxation component (W_3, τ_3) at film temperatures substantially above T_g (153 °C). These observations suggest the presence of one discrete/homogeneous microenvironment about the chromophore. As the temperature is lowered further toward T_g, β decreases, signaling additional relaxation processes. The data in this temperature range (149–137 °C), however, remain well modeled by the theoretically derived bi-exponential form. Below T_g, the multiplicity of chromophore microenvironments increases dramatically, as indicated by a decrease in β as well as deteriorating fits to eq 23. The broadening of the distribution of rotational relaxation rates arises because the locally differing microenvironments of the chromophore relax at different rates. This kinetic matrix effect manifests itself as a deviation from first-order kinetics. Thus, the KWW β parameter is actually providing us with a measure of the chromophore relaxation dynamics deviation from first-order kinetic behavior.

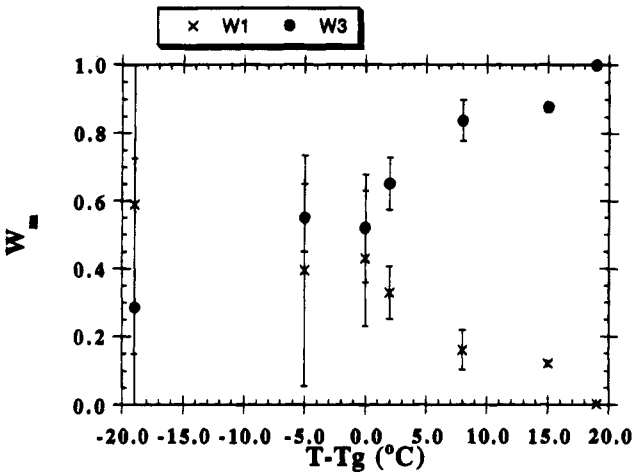

Figure 8. Plot of W_1 and W_3 (Table 2), the fraction of dipoles undergoing slow and fast relaxation processes, respectively, as a function of temperature from T_g for 36% functionalized, contact-poled (*S*)-NPP-PHS. The coefficients were obtained by a nonlinear least-squares fit of the data to eq 23.

One possible interpretation of these results is based on free volume considerations. Specifically, W_3 and W_1 may be viewed as the fractional contribution of the total decay from the fast and slow motion/decay components. Therefore, the fraction of fast and slow second-harmonic signal decay can be used to characterize the relaxation kinetics. The minimum microvoid volume (free volume) required for rotational diffusion about the dipole moment axis for NPP can be estimated by considering rotation of the chromophore which has a volume of ~190 Å³. Clearly then, the minimum microvoid volume required for movement of the rigid dipole must exceed 190 Å³. According to Cohen and Grest's[53–55] free volume model, microvoids having greater than the critical volume and termed "liquid-like", while islands with less than this volume are termed "solid or glasslike" cells. Molecular displacement or rotation is believed to occur only in the "liquid-like" cells. It is possible, therefore,

Table 3. Above-T_g Relaxation (Post Contact Poling) SHG Kinetic Parameters for 36% Functionalized (*S*)-NPP-PHS (Decay Transients Presented in Figure 7)

temp (°C)	$10^{-3}D_R$ (rad^2/s)[a]	τ_3 (s)[b]
134	2.3(0.2)	36.2
137	2.7(0.1)	30.9
142	4.8(0.3)	17.4
149	8.7(0.3)	9.6
153	9.7(0.05)	8.6

[a] D_R values obtained by nonlinear least-squares fitting of data (Figure 7) to eq 23. [b] Obtained via eq 42.

by employing a biphasic analysis, such as that provided by eq 23, to estimate the fraction of dipoles occupying "liquid-like" regions (*i.e.*, the W_3 fraction) and "glasslike" regions (*i.e.*, the W_1 fraction) in the polymer matrix. For example, for 36% functionalized (*S*)-NPP-PHS poled at 153 °C, essentially 100% of the dipoles apparently occupy "liquid-like" regions. This interpretation, however, is not required to explain bi-exponential behavior for rotational relaxation, which arises directly from free angular diffusion (eq 23).

Temperature Dependence of Field-Free SHG Decay above T_g. An examination of decay transients using eq 23 yields the hydrodynamic parameter, D_R. The rotational diffusion coefficients found for 36% functionalized (*S*)-NPP-PHS above T_g, summarized in Table 3, are substantially smaller than that previously reported by Dhinojwala et al.[50] for guest–host systems ($D_R \approx 2.5 \times 10^{-3}$ to 100 rad^2 s^{-1}), indicating that the guest–host systems have less constrained orientational freedom than do side-chain functionalized polymers. In addition, the derived diffusivities for the present covalently appended chromophores exhibit significantly less temperature sensitivity above T_g (Table 3) than the simple dispersed chromophore-polymer systems.[50] These results quantitatively underscore the benefit of tethering the NLO chromophore to the polymer backbone as a means of reducing the dipolar relaxation rate and thereby stabilizing the field-induced second-order nonlinearity.

From the rotational diffusion coefficients, values of the fast relaxation time, τ_3, the dominant decay component above T_g, can be calculated via the expression

$$\tau_3 = \frac{1}{k_3} = \frac{1}{12D_R} \tag{42}$$

The resultant relaxation times for 36% functionalized (*S*)-NPP-PHS, also summarized in Table 3, show that τ_3 decreases as the temperature of the sample approaches T_g. These results are consistent with the increased segmental mobility and local free volume expected when the polymer is heated to or above T_g. These induced changes in the polymer matrix above T_g facilitate chromophore rotation, as reflected in the increasing diffusivity parameters (Table 3).

The temperature-dependent behavior of the experimentally recorded decay transients above T_g can be examined further using the Williams–Landel–Ferry, WLF, equation[56] where τ is the relaxation time (here, τ_3) and C_1 and C_2 are empirical "constants" the magnitudes of which,

$$\log \frac{\tau(T)}{\tau(T_g)} = \frac{-C_1(T - T_g)}{C_2 + T - T_g} \tag{43}$$

determined by fitting various data collected on a large number of polymers, are frequently estimated to be

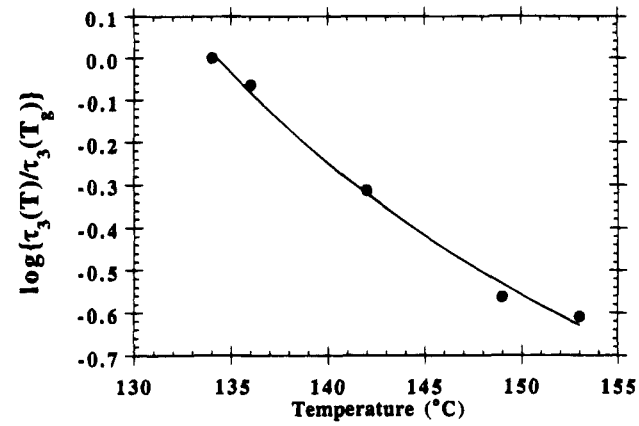

Figure 9. Temperature dependence of τ_3 above T_g for contact-poled 36% functionalized (*S*)-NPP-PHS. The solid line is the nonlinear least-squares fit to the WLF equation (eq 43).

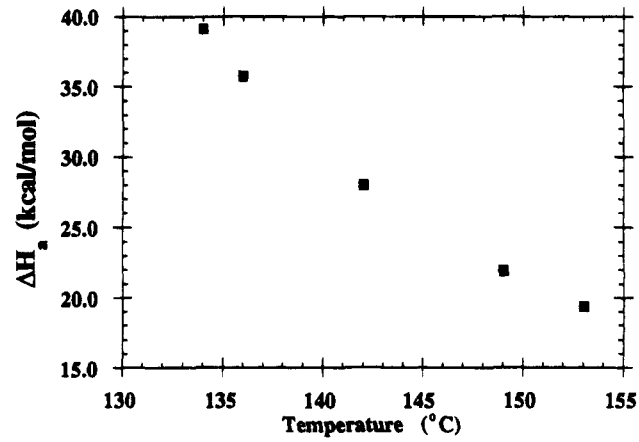

Figure 10. Temperature dependence of the apparent activation enthalpies, ΔH_a, calculated using eq 44, describing the above-T_g relaxation dynamics of 36% functionalized (*S*)-NPP-PHS.

17.44 and 51.60 °C, respectively. (The actual values of C_1 and C_2 *vary greatly* from one polymer to another, however, and must be measured for the specific polymer of interest.)[57] Since the WLF equation is generally only valid above T_g, the present analysis was applied only to the decay transients collected between 134 and 153 °C (Figure 9). The WLF parameters obtained from such an analysis are $C_1 = 1.94$ and $C_2 = 39.1$ K. It has been suggested that the differences might be expected since the "universal" WLF parameters describe the macroscopic relaxation behavior of a polymer, whereas in the present case the local relaxation, *i.e.*, the actual free volume around the chromophore, is predominant.[57] From these WLF parameters, an apparent enthalpy of activation, ΔH_a, for viscoelastic flow can be calculated from the expression[29,58]

$$\Delta H_a = \frac{2.303RC_1C_2T^2}{(C_2 + T - T_g)^2} \tag{44}$$

where R is the ideal gas constant and all other variables are as previously defined. The derived activation enthalpies increase rapidly with decreasing temperature (Figure 10) from a maximum value of 39.0 ± 4.0 kcal/mol at T_g (134 °C) to a minimum of 19.0 ± 2.0 kcal/mol at 153 °C. Note that the ΔH_a values found in this analysis (using the 3-D rotational diffusion-derived relaxation times, τ_3) agree well with the results reported previously[24] which used the KWW-derived relaxation times (44.5 ± 4.5 kcal/mol at 134 °C and 10.8 ± 1.1 kcal/

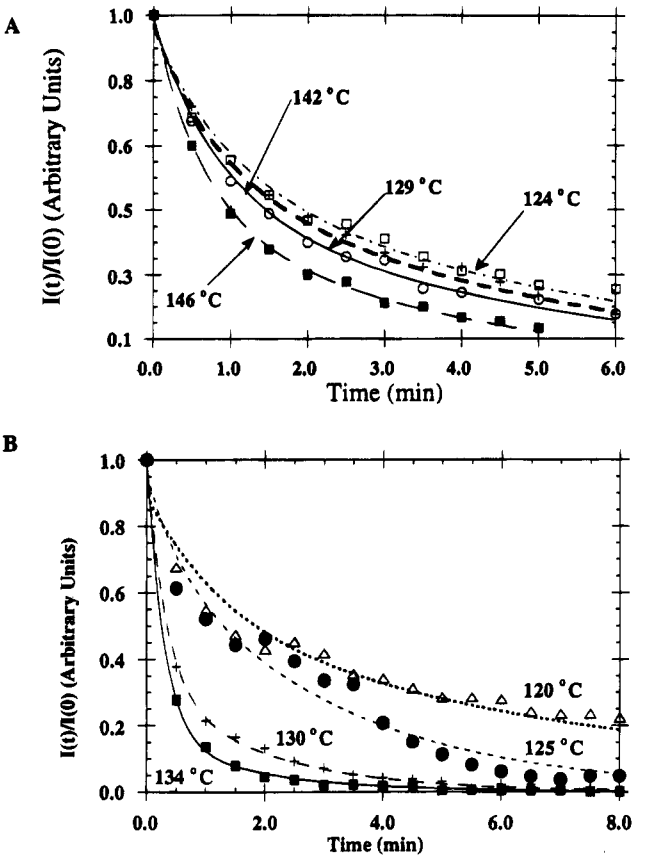

Figure 11. SHG decay transients collected at various temperatures at and below T_g, for contact-poled (E_p = 0.83 MV/cm; t_{E_p} = 20 min) 12% functionalized (*S*)-NPP-PHS (T_g = 146 °C). Lines are nonlinear least-squares fits of the data to eq 23. Error bars on the data are equal to or less than the symbol dimensions. (B) SHG decay transients collected at various temperatures at and below T_g, for contact-poled (E_p = 1.25 MV/cm; t_{E_p} = 20 min) 36% functionalized (*S*)-NPP-PHS (T_g = 134 °C). Lines are nonlinear least-squares fits of the data to eq 23. Error bars on the data are equal to or less than the symbol dimensions.

mol at 153 °C). The nonlinear dependence of the activation enthalpy on temperature has been postulated to arise from cooperative intermolecular motions, specifically, large scale cooperative main chain movement.[59] The nature of the motion occurring above T_g has been investigated previously in substituted polystyrenes (PS) using a variety of methods, including dielectric spectroscopy and ^{13}C NMR.[60-62] Although the exact nature of these motions is not well understood, it is believed that for PS and its derivatives, they principally involve large amplitude movement in the phenyl rings (e.g., ring flips) coupled to motion of the main chain carbons which relieves local steric strain.[60,61]

Temperature Dependence of Field-Free SHG Decay below T_g. In the glassy state, conformational changes of the polymer backbone involving multiple atoms are largely arrested and only rotational or librational rearrangements of the side groups are important.[1] As demonstrated previously,[24] the temperature-dependent behavior of the sub-T_g relaxation processes for NPP-PHS obeys the Arrhenius law,

$$\ln(k) = \ln(A) - \frac{E_a}{RT} \tag{45}$$

with temperature-independent activation energy, E_a. The impact of increasing chromophore concentration on the temperature dependence of the post electric field

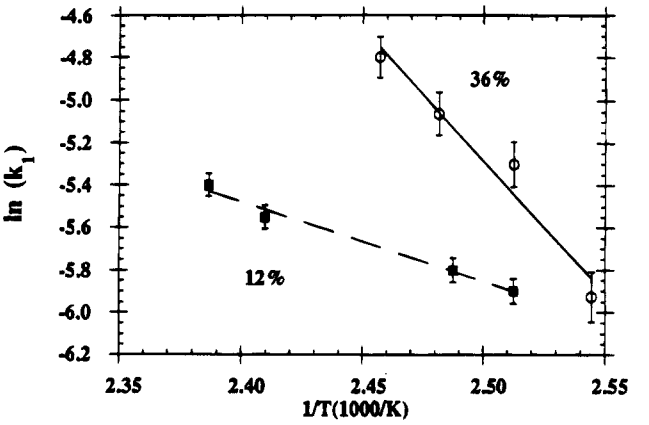

Figure 12. Arrhenius plots describing temperature-dependent dipolar relaxation in contact-poled, glassy state 12% and 36% functionalized (*S*)-NPP-PHS films. The lines are least-squares fits to eq 45.

Table 4. Glassy State Kinetic Parameters

temp (°C)	$10^3 D_R$ (rad²/s)	τ_1 (s)	τ_3 (s)
a. For 36% Functionalized (*S*)-NPP-PHS[a]			
134	4.11(0.15)	120.0	20.3
131	3.17(0.33)	158.0	26.3
128	2.58(0.27)	194.0	32.3
122	1.35(0.20)	375.0	61.2
b. For 12% Functionalized (*S*)-NPP-PHS[b]			
146	2.33(0.25)	214.6	35.8
138	1.83(0.27)	273.2	45.5
131	1.48(0.22)	337.8	56.3
125	1.32(0.20)	379.8	63.1

[a] Determined by fitting experimental SH relaxation transients (Figure 11B) to eq 23. [b] Determined by fitting experimental SH relaxation transients (Figure 11A) to eq 23.

Table 5. Comparison of Kinetic Parameters for (*S*)-NPP-PHS at Two Functionalization Levels

functionalization level (%)	A[a] (s^{-1})	E_a[a] [kcal/mol (kJ/mol)]	$\Delta S^{\ddagger}$[b] [J/(K mol)]	$\Delta G^{\ddagger}$[b] (kJ/mol)
12	0.34×10^2	7.46 (32.0)	−553.5	220.2
36	1.46×10^{11}	24.6 (103.0)	−129.0	151.3

[a] Values obtained from Arrhenius plots (Figure 12). Estimated uncertainties, ±10%. [b] Calculated at 125 °C using transition state theory, $k_3 = (\kappa T/h)e^{(\Delta S^{\ddagger}/R)}e^{(-E^{\ddagger}_a/RT)}$. Estimated uncertainties, ±10%.

relaxation (randomization) was evaluated below T_g (in the glassy state). Arrhenius plots for 12% and 36% functionalized (*S*)-NPP-PHS were constructed using nonlinear least-squares fits of SHG decay transients to eq 23 (Figure 12). The 3-D rotational diffusion model was used for this analysis. As demonstrated above, such an analysis yields the diffusivity parameter, D_R, and thus, the fast relaxation time, τ_3, and the corresponding rate constant, k_3 (eq 42). In a similar fashion, the slow relaxation component, τ_1, and the corresponding rate constant, k_1, can be calculated by

$$\tau_1 = \frac{1}{k_1} = \frac{1}{2D_R} \tag{46}$$

The resultant diffusivities and the slow and fast relaxation times are summarized in Table 4. Note that although the values of the fast and slow relaxation components differ by a factor of 6, their temperature-dependent behavior should not.

Arrhenius plots for both 12% and 36% functionalized (*S*)-NPP-PHS are presented in Figure 12, and the resultant activation energies (E_a) and frequency factors (A) are summarized in Table 5. The activation energies found here are comparable to those reported for other

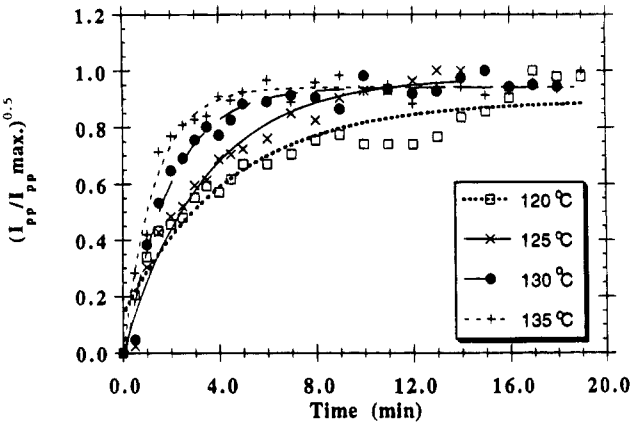

Figure 13. Second harmonic growth curves for contact-poled 36% functionalized (*S*)-NPP-PHS at a series of temperatures (E_p = 1.25 MV/cm; t_{E_p} = 20 min; $u \sim 0.5$). Lines represent nonlinear least-squares fits to eq 37. The poling field was turned on at $t = 0$.

Table 6. Summary of Kinetic Parameters Derived for Contact-Poled 36% Functionalized (*S*)-NPP-PHS Film Growth Profiles Fit to Eq 37[a]

temp (°C)	N	W_1	D_R (rad²/min)	goodness of fit
120	0.89(0.03)	0.76(0.05)	0.11(0.02)	0.962
125	0.98(0.02)	0.98(0.03)	0.14(0.01)	0.989
130	0.94(0.01)	0.99(0.04)	0.26(0.02)	0.988
135	0.94(0.01)	0.96(0.03)	0.38(0.02)	0.989

[a] Numbers in parentheses are standard deviations on the respective fit parameters.

systems[63] and are typical of those observed for small molecular side-group motions (for which activation energies are usually ≥20 kcal/mol for highly polar side groups[64]). Moreover, these values compare favorably with those reported for polystyrene measured by static and dynamic mechanical techniques. Specifically, activation energies of 30–33 kcal/mol have been determined for PS β relaxation by dielectric spectroscopy and are postulated to arise from local mode relaxation.[30,31] Thus, our analysis indicates that sub-T_g SHG can be used to probe secondary relaxations, *e.g.*, side-group reorientation on a dynamically quiescent main chain.

Kinetic Analysis of Experimental Field-on/ Growth of $\langle\cos^3\theta\rangle$. The time dependence of the increase in the SHG $\langle\cos^3\theta\rangle$ ($\propto d_{33}$) coefficient for contact-poled 36% functionalized (*S*)-NPP-PHS, normalized to the plateau values, is presented in Figure 13. Parameters obtained from the nonlinear least-squares fit of the data to eq 37, the growth function for low field strengths, are summarized in Table 6. The experimental data show excellent agreement with the theoretically predicted mono-exponential function derived for SHG growth/dipolar alignment, except at the lowest temperature transient, 120 °C. The three higher temperature transients agree not only with theoretical predictions but also with prior analysis of the same growth transients using the empirical KWW function.[24] Recall that this analysis yielded a KWW β parameter of 1.0 (single exponential behavior) for the two highest temperature trials. These results demonstrate that the chromophore alignment process between T_g and 125 °C is well modeled as simple rotational diffusion of a rigid rotor in the presence of an external dc field. The discrepancies which arise at the lowest temperature indicate deficiencies in this simple model, *i.e.*, deviation from simple first-order kinetics. It is possible that these deviations reflect changes occurring in the polymer matrix. More specifically, as temperatures fall below

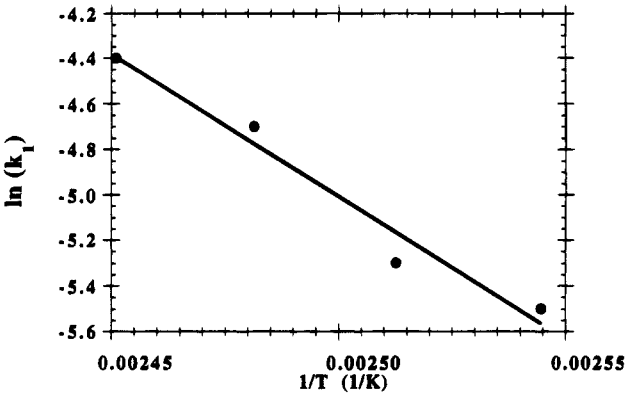

Figure 14. Arrhenius plot of temperature-dependent dipolar alignment (field-on) for glassy state 36% functionalized (*S*)-NPP-PHS. The line represents the least-squares fit of the data to eq 45.

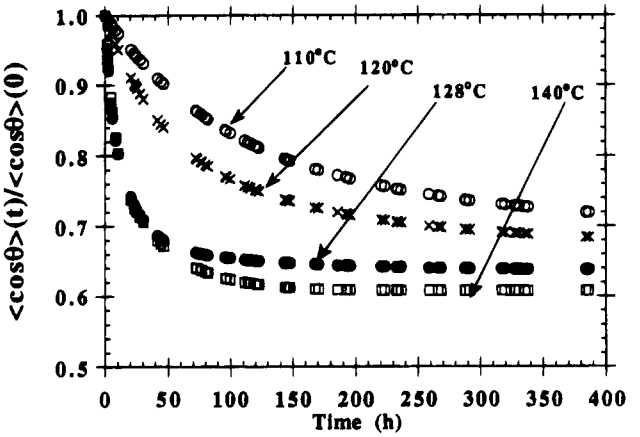

Figure 15. $\langle\cos\theta\rangle$ transients determined by experimental measurements of d_{33} and d_{31} and by applying eq 47 for 36% functionalized (*S*)-NPP-PHS films which were corona poled (+5.0 kV; t_{E_p} = 30 min) at various temperatures above and below T_g and then cooled to room temperature prior to field cessation. Transients were collected at 25 °C.

T_g, the chromophore population shifts toward occupation of "solid/glasslike" regions which require structural adaptation of the polymer matrix to permit chromophore alignment. Macroscopically, this is reflected as two distinct processes, an initial fast response, caused by the fraction of chromophores able to undergo local, side-chain rotation, and a slower response which requires global movement of the polymer.

The temperature-dependent behavior of induced SHG activity during electric field poling can be examined further *via* an Arrhenius plot (Figure 14). From the rotational diffusion coefficients (Table 6) the kinetic growth times, τ_1 ($^1/_2D_R$) can be determined. The activation energy, E_a, for the field-on poling dynamics is 24.8 ± 2.5 kcal/mol, in excellent agreement with that determined for the field-off relaxation process (24.6 ± 2.5 kcal/mol; Table 5). Agreement in activation energies for both field-on and field-off dynamics has been reported for one guest-host polymer.[65]

Kinetic Analysis of Experimental Field-Free Decay of $\langle\cos\theta\rangle$. Independent measurement of the post electric field relaxation behavior of d_{33} and d_{31} permits examination of the experimental decay characteristics of $\langle\cos\theta\rangle$. The first moment is related to the two measured SHG coefficients according to

$$\frac{\langle\cos\theta\rangle(t)}{\langle\cos\theta\rangle(0)} = 2\frac{d_{31}(t) + d_{33}(t)}{d_{31}(0) + d_{33}(0)} \qquad (47)$$

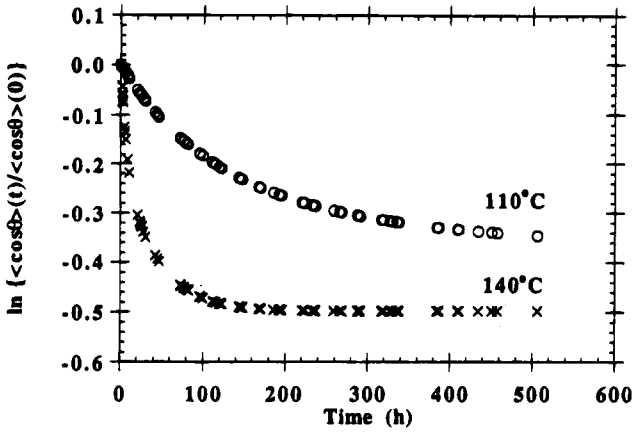

Figure 16. $\langle \cos \theta \rangle$ decay transients presented in Figure 15 for 36% (*S*)-NPP-PHS plotted as ln $\langle \cos \theta \rangle$ to emphasize multi-exponential decay character.

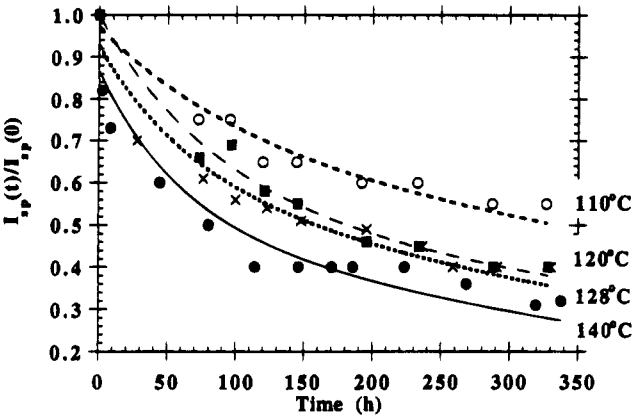

Figure 17. SHG decay transients collected at various temperatures above and below T_g, for corona-poled (+5.0 kV; t_{E_p} = 30 min) 36% functionalized (*S*)-NPP-PHS films. Films were cooled to room temperature prior to field removal and all data collected at 25 °C. Lines are nonlinear least-squares fit of data to eq 29.

The relaxation behavior of the derived normalized $\langle \cos \theta \rangle$ temperature-dependent transients for 36% functionalized (*S*)-NPP-PHS are presented in Figure 15. Contrary to expectations, for low fields, it was found that none of these transients can be fit (Figure 16) to the single exponential function, eq 24 predicted by the three-dimensional rotational diffusion model. The discrepancy is illustrated in Figure 16 for the highest (140 °C) and lowest (110 °C) transient studies. The origin of this discrepancy is unclear; it may, however, indicate the appearance of additional relaxation modes due to the time-dependent heterogeneity in the local microenvironment. Experimental deviations from the mono-exponential behavior theoretically predicted for $\langle \cos \theta \rangle$ have been previously reported by Meyrueix et al. on other chromophore-functionalized polymers.[66,67]

Kinetic Analysis of Experimental Field-Free Decay of d_{31}. The validity of the theoretically predicted field-free d_{31} relaxation function (eq 29) was examined using SHG decay data collected on corona-poled 36% (*S*)-NPP-PHS films. At all temperatures examined, the experimental data *could not* be convincingly fit to eq 29, the generalized 3-D decay function. The data, however, could be fit to the functional form derived from the 2-D model (eq 15), as demonstrated in Figure 17. The temperature dependences of W_1 and W_3 are presented in Table 7, and for all temperatures studied, W_1 exceeds W_3, in qualitative agreement with theoretical expectations (Table 8).

Table 7. Summary of Fit Parameters Obtained for d_{31} Relaxation Dynamics of 36% Functionalized (*S*)-NPP-PHS Collected at Various Temperatures[a]

temp (°C)	W_3	W_1	$10^3 D_R$ (rad²/min)	goodness of fit
110	0.26(0.04)	0.71(0.02)	1.10(0.06)	0.974
120	0.42(0.04)	0.57(0.03)	1.30(0.06)	0.991
128	0.31(0.05)	0.62(0.02)	1.70(0.13)	0.970
140	0.34(0.05)	0.53(0.03)	1.97(0.2)	0.962

[a] Parameter obtained by fitting data (Figure 17) to eq 15.

Table 8. Theoretically Predicted Changes in the Pre-Exponential Coefficients As Determined by Computer-Simulated Electric Field Poling Using the Two-Dimensional Rotational Diffusion Model

temp (°C)	field strength, E_p (V/m)	diffusion coeff, D_R (rad²/s)	W''_1[a]	W''_3[a]
130	2.5×10^7	1.5×10^{-5}	1.00	-4.58×10^{-4}
130	2.5×10^8	1.5×10^{-5}	1.00	−0.004
50	2.5×10^8	1.5×10^{-5}	1.07	−0.072

[a] Coefficients calculated by insertion of appropriate probability coefficients into eqs 14 and 15. The $f_1(0)$ and $f_3(0)$ values used were those theoretically determined immediately prior to field cessation.

Conclusions

Theoretical modeling and computer simulations of the time-varying dynamics of an NLO chromophore dipole interacting with an externally applied electric poling field have been performed using the Smoluchowski equation. The dynamic 2-D rotational diffusion model predicts that the field-on equilibrium ratio of the two second-harmonic coefficients, d_{33}/d_{31} (R), will be 6.0. The corresponding 3-D model predicts an R value of 3.0, in agreement with that obtained using a static statistical–mechanical model. Comparison of the computer-simulated transients of the second-harmonic coefficients using the 2- and 3-D models indicates that the growth and decay dynamics should proceed more slowly in two-dimensional space than in three, as might be expected by simple geometric considerations. After electric field removal, both 2-D and 3-D models predict mono-exponential $\langle \cos \theta \rangle$ decay and bi-exponential d_{33} and d_{31} decay. In both models, the field-on dynamics of chromophore alignment are not conveniently predicted analytically. Approximations predict that at low field strengths, d_{33} signal growth is single exponential, and with increasing field strength, the behavior is complex, being more accurately characterized as bi-exponential.

The analytic functions derived by employing the rotational diffusion model have been applied to experimental SHG transients obtained on the prototypical side-chain chromophore-functionalized polymer (*S*)-NPP-PHS. Specifically, at the above T_g, the rotational reorientation (field-off SHG) dynamics of the d_{33} coefficient are well described by the bi-exponential function predicted by the 3-D model. Conformance to a bi-exponential function might at first be argued to indicate that at these temperatures, the free volume about the chromophoric probe may be viewed as having a bimodal distribution, *i.e.*, liquid-like regions of high rotational mobility and solidlike regions of low mobility. No such assumption is needed, however, since the rotational diffusion model, itself, predicts a bi-exponential. Below T_g, the d_{33} relaxation dynamics no longer obey a simple Smoluchowski equation, as indicated by the increasingly poor fits to the predicted bi-exponential function for the 3-D model. Thus, in the glassy state (sub-T_g), a relaxation mechanism of greater complexity must be invoked, leading to more accurate modeling of the dynamics by

the KWW function. Comparison of the curve fits of the decay/growth dynamics using both the rotational diffusion framework and the empirical KWW function demonstrates that the phenomenological KWW model yields descriptions of comparable accuracy, with the KWW β parameter providing an indicator of the deviation from first-order kinetic behavior. The increasing heterogeneity of the chromophore microenvironment (the polymer matrix) is not the only contribution to the breakdown of the rotational diffusion controlled dynamics. Consideration must also be given to specific interactions both of the NLO-phore dipole with the matrix and between the NLO-phores themselves.

The temperature dependence of dipolar relaxation above T_g is not Arrhenius-like; however, it can be modeled well using the Williams–Landel–Ferry equation. The temperature-dependent activation enthalpy is suggested to be correlated with phenyl ring movement coupled to main chain motion. Below T_g, the temperature dependence of the time constants associated with the reorientation process was found to be Arrhenius-like. The kinetic parameters obtained are suggested to be correlated with rotational and librational motions of the chromophore.

The rotational reorientational (field-off, SHG decay) kinetics of the d_{31} second-harmonic coefficient and first moment of cos θ were also studied. The d_{31} dynamics could be modeled fairly accurately using the theoretical expression predicted by a 2-D model, whereas $\langle\cos\theta\rangle$ could not be modeled using the bi-exponential functional forms derived from either model. The orientation (field-on, SHG growth) kinetics for d_{33} were also investigated and accurately approximated using theoretical expressions derived from a 3-D model. The activation energy derived for glassy state polarization was found to be indistinguishable from that found for depolarization. The more heavily functionalized (36%) polymer relaxes more rapidly, perhaps due to plasticizing by the side chains, since T_g for 36% (*S*)-NPP-PHS polymer is lower than for the 12% (*S*)-NPP-PHS; the more rapid relaxation is in accord with expectations based on the WLF equation.

Unlike the majority of available spectroscopic methods which provide information solely on the second-order Legendre polynomial, $P_2(\cos\theta)$ (*e.g.*, NMR, Kerr effect), SHG can provide information simultaneously on both the first- and third-order Legendre polynomials, $P_1(\cos\theta)$ and $P_3(\cos\theta)$. It is apparent, however, from this work that the interpretation of relaxation spectroscopic results from SHG techniques is, at this stage, substantially more complex than suggested by a simple Smoluchowski equation. Further development of appropriate models for viscoelastic relaxations monitored by SHG techniques is still in its infancy, requiring additional work to fully explore its potential as a relaxation spectroscopy. Although the present study focused on the time evolution of the SHG response and its constituent moments, the models and the modifications thereof are suitable for extension to other second-order effects (*i.e.*, electro-optic effect) or to the study of birefringence (Kerr effect). From a technological viewpoint, it is desirable to stabilize the orientation achieved in poled polymers for very long times, even during high-temperature excursions.[3,4,68] Methods implemented include functionalization, cross-linking, and physical aging.[3,4,68] In the context of our treatment here, these all have the effect of substantially reducing the rotational diffusion coefficients, and thereby reducing the decay of d_{33} and d_{31}.

The rotational diffusion model used here, with no polymer-based potentials or interchromophore interactions, is clearly oversimplified. It cannot deal with situations (such as host–guest systems) in which translational diffusion (which is likely of minor importance here[69]) occurs and clearly will fail for short times or for temperatures substantially below T_g, where barriers become important.

For viscoelastic materials like the polymers examined here, one expects a spectrum of local relaxation times. It is then reasonable to expect that the description of relaxation of a dipolar probe chromophore will also show a form of hierarchical behavior, with each time scale characterized by a viscous drag arising from motion on faster time scales, and by an elastic potential term due to relaxation on slower relaxation time scales. Analysis of such a model[32] reveals that the relaxation is expected to be single exponential at short times and again at very long times, but of KWW (stretched exponential) type at intermediate times. This is substantially different from the results of the simple rotational diffusion models presented here, which yield multiple exponential decay. While the actual fitting to a KWW or bi-exponential form can often be comparably accurate, the physics of the relaxation process will vary substantially, since the former corresponds to a distribution of relaxation times and a memory kernel form for the local friction, while the latter results from a simple rotational diffusion (Smoluchowski) picture. Measurements of relaxation at very short times should be useful in trying to distinguish these behaviors. Analysis of measured d_{33} and d_{31} response with that sort of relaxation model has yet to be completed.

Acknowledgment. The authors would like to thank Prof. H. Mayne and Dr. M. Thachuk for many helpful discussions and Prof. G. Wong for collaboration on SHG measurements. We thank AFOSR (contract 93-1-0114) and the Northwestern Materials Research Center (NSF Materials Research Center Program grant DMR9120521) for financial support. M.A.F. acknowledges IBM Corp. for a Cooperative Graduate Fellowship.

Appendix A

An analytic solution to the 2-D rotational diffusion problem (eq 6) can be found by expanding $f(\theta,t)$ in a Fourier series,

$$f(\theta,t) = \sum_m f_m(t)\, e^{(im\theta)} \tag{A1}$$

Substituting eqs 3 and A1 into eq 6 and using known trigonometric identities gives

$$\sum_m \frac{df_m(t)}{dt} e^{(im\theta)} = \sum_m f_m(t)\left[-D_R m^2 e^{(im\theta)} + \frac{D_R\mu E}{2kT} m e^{(i(m+1)\theta)} - \frac{D_R\mu E}{2kT} m e^{(i(m-1)\theta)}\right] \left[+\frac{D_R\mu E}{2kT} e^{(i(m+1)\theta)} + \frac{D_R\mu E}{2kT} e^{(i(m-1)\theta)}\right] \tag{A2}$$

The time-dependent probability coefficients, $f_m(t)$, are obtained by multiplying both sides of eq A2 by $e^{-im'\theta}$ and imposing the orthogonality condition[34,35]

$$\int_0^{2\pi} e^{i(m-m')\theta}\, d\theta = 2\pi\delta_{mm'} \quad \text{where } m = ..., -2, -1, 0, 1, 2, ... \quad \text{(A3)}$$

to yield the following recurrence relationship

$$\frac{df_{m'}(t)}{dt} = \frac{D_R\mu E}{2kT} m' f_{m'-1}(t) - D_R m'^2 f_{m'} - \frac{D_R\mu E}{2kT} m' f_{m'+1}(t) \quad \text{(A4)}$$

Thus, $f_{m'}$, is coupled to both $f_{m'-1}$ and to $f_{m'+1}$.

Once the differential equation for the time-dependent coefficients (eq A4) is solved, the temporal behavior of the second-harmonic coefficients, d_{33} and d_{31}, may be determined through calculation of the polar order parameters, $\langle\cos^3\theta\rangle$ and $^1/_2[\langle\cos\theta\rangle - \langle\cos^3\theta\rangle]$. In two-dimensions, the averages become

$$\langle z(\theta)\rangle_{2D} = \frac{\int_0^{2\pi} f(\theta,t)\, z(\theta)\, d\theta}{\int_0^{2\pi} f(\theta,t)\, d\theta} \quad \text{(A5)}$$

where $z(\theta)$ is $\cos\theta$ or $\cos^3\theta$. Substitution of the expression for the time-dependent probabilities of θ, eq A1, into eq A5 and application of the orthogonality condition (A3) gives

$$\langle\cos\theta\rangle_{2D} = \frac{f_{-1} + f_1}{2f_0} \quad \text{(A6)}$$

$$\langle\cos^3\theta\rangle_{2D} = \frac{f_{-3} + 3f_{-1} + 3f_1 + f_3}{8f_0} \quad \text{(A7)}$$

Appendix B

The appropriate eigenfunctions for a three-dimensional system of axial symmetry are the Legendre polynomials. By substituting both Legendre's equation expressed in terms of differentiation with respect to θ (eq B1),[46]

$$\frac{1}{\sin\theta}\frac{\partial}{\partial\theta}\left(\sin\theta\frac{\partial P_m(\cos\theta)}{\partial\theta}\right) = -m(m+1)P_m(\cos\theta) \quad \text{(B1)}$$

and the expression for the time-dependent probability of θ,

$$f(\theta,t)\sum_m f_m(t)\, P_m(\cos\theta) \quad \text{(B2)}$$

back into the rotational diffusion equation, the following expression is obtained:

$$\sum_m f_m(t)\left[-m(m+1)P_m(\cos\theta) + \frac{\mu E}{kT}\left((\cos^2\theta - 1)\frac{\partial P_m(\cos\theta)}{\partial\cos\theta} + 2\cos\theta\, P_m(\cos\theta)\right)\right] \quad \text{(B3)}$$

Re-expressing the first derivative of a Legendre polynomial as,[47]

$$\frac{\partial P_m(\cos\theta)}{\partial\cos\theta} = \frac{-m\cos\theta\, P_m(\cos\theta) + mP_{m-1}(\cos\theta)}{1 - \cos^2\theta} \quad \text{(B4)}$$

multiplying both sides by $P_{m'}(\cos\theta)$, and applying the orthogonality condition,[48]

$$\int_{-1}^{1} P_m(\cos\theta)P_{m'}(\cos\theta)\, d\cos\theta = \frac{2\delta_{mm'}}{2m+1} \quad \text{where } m = 0, 1, 2, 3, ... \quad \text{(B5)}$$

results in a diffusion equation of the following form:

$$\frac{1}{D_R}\frac{df_{m'}(t)}{dt}\frac{2}{2m'+1} = -m'(m'+1)\frac{2}{2m'+1}f(t)_{m'} - \frac{\mu E 2(m'+1)}{kT 2m'+3}f(t)_{m'+1} + \frac{\mu E}{kT}(m'+2)\sum_m f(t)_{m'}\int_{-1}^{1} P_m P_1 P_{m'}\, d\cos\theta \quad \text{(B6)}$$

The solution to the remaining integral over the triple product of Legendre polynomials can be evaluated through the use of 3-j symbols.[49] From this, the following recursion formula may be derived, from which the time-dependent coefficients, $f_m(t)$, are found,

$$\frac{df_{m'}(t)}{dt} = \frac{5D_R\mu E}{kT}\left(\frac{m'+1}{2m'+3}\right)f_{m'+1}(t) - D_R m'(m'+1)f_{m'}(t) + \frac{2D_R\mu E}{kT}\left(\frac{m'(m'+1)}{2m'-1}\right)f_{m'-1}(t) \quad \text{(B7)}$$

Once the differential equation for the time-dependent coefficients (eq B7) is solved, the temporal behavior of the pertinent second-harmonic coefficients, d_{33} and d_{31}, may be determined through the orientational order parameters $\langle\cos^3\theta\rangle$ and $^1/_2[\langle\cos\theta\rangle - \langle\cos^3\theta\rangle]$. The first and third moments of $\cos\theta$ can be found by employing an average analogous to that introduced in eq A5

$$\langle z(\theta)_{3D}\rangle = \frac{\int_{-1}^{1} f(\theta,t)\, z(\theta)\, d\cos\theta}{\int_{-1}^{1} f(\theta,t)\, d\cos\theta} \quad \text{(B8)}$$

where $z(\theta)$ is either $\cos^3\theta$ or $\cos\theta$. The third moment, $\langle\cos^3\theta\rangle$, can be found by substitution of the rearranged third-order Legendre polynomial, $P_3(\cos\theta)$,

$$\cos^3\theta = \frac{2P_3(\cos\theta) + 3P_1(\cos\theta)}{5} \quad \text{(B9)}$$

and the expression for the time-dependent probabilities of θ, eq B2, into eq B8. After application of the orthogonality relationship, eq B5, the third moment can be written in terms of the calculated probabilities,

$$\langle\cos^3\theta\rangle = \frac{2f_3 + 7f_1}{35f_0} \quad \text{(B10)}$$

By using a similar procedure, $\langle\cos\theta\rangle$ can be written in the following form

$$\langle\cos\theta\rangle = \frac{f_1}{3f_0} \quad \text{(B11)}$$

References and Notes

(1) *Local Dynamics in Amorphous Polymers*; Jones, A. A., Ed.; John Wiley & Sons: New York, 1989; pp 247–271.
(2) Ewen, B. *Adv. Mater.* **1993**, *5*, 260–266.
(3) Marks, T. J.; Ratner, M. A. *Angew. Chem., Int. Ed. Engl.*, in press.
(4) *Optical Nonlinearities in Chemistry*; Burland, D. M., Ed.; *Chem. Rev.* **1994**, *94*.

(5) *Molecular Nonlinear Optics: Materials, Physics, and Devices*; Zyss, J., Ed.; Academic Press: Boston, 1993.
(6) *Polymers for Lightwave and Integrated Optics Technology and Applications*; Nornak, L. A., Ed.; Marcel Dekker, Inc.: New York, 1992.
(7) Prasad, P. N.; Williams, D. J. *Nonlinear Optical Effects in Molecules & Polymes*; John Wiley & Sons: New York, 1991.
(8) *Organic Molecules for Nonlinear Optics and Photonics*; Messier, J., Kajzar, F., Prasad, P., Eds.; Kluwer Academic Publishers: Boston, 1991; Vol. 194.
(9) *Materials for Nonlinear Optics: Chemical Perspectives*; Marder, S. R., Sohn, J. E., Stucky, G. D., Eds.; American Chemical Society: Washington, DC, 1991; Vol. 455.
(10) *Nonlinear Optical Properties of Organic Materials VI*; Möhlmann, G. R., Ed.; SPIE Proceedings; SPIE: 1993; p 2025.
(11) *Nonlinear Optical Properties of Organic Materials V*; Williams, D. J., Ed. SPIE Proceedings; 1992; p 1775.
(12) Williams, G.; Watts, D. C. *Trans. Faraday Soc.* **1970**, *66*, 80–85.
(13) Kohlrausch, R. *Ann. Phys. (Leipzig)* **1847**, *12*, 393–395.
(14) Firestone, M. A.; Park, J. W.; Minami, N.; Marks, T. J.; Ratner, M. A.; Lin, W.; Wong, G. K. *Macromolecules* **1995**, *28*, 2247–2259.
(15) Meredith, G. R.; Van Dusen, J. G.; Williams, D. J. *Macromolecules* **1982**, *15*, 1385–1389.
(16) Meredith, G. R.; Van Dusen, J. G.; Williams, D. J. In *Nonlinear Optical Properties of Organic and Polymeric Materials*; Williams, D. J., Ed.; American Chemical Society: Washington, DC, 1983; Vol. 233, pp 109–133.
(17) Singer, K. D.; Kuzyk, M. G.; Sohn, J. E. *J. Opt. Soc. Am. B* **1987**, *4*, 968–975.
(18) Van der Vorst, C. P. J. M.; Pickens, J. J. *J. Opt. Sci. Am. B* **1990**, *4*, 918–922.
(19) van der Vorst, C. P. J. M.; Horsthuis, W. H. G.; Möhlmann, G. R. In ref 6, pp 365–395.
(20) Wang, C. H. *J. Chem. Phys.* **1993**, *98*, *3457*–3461.
(21) Guan, H. W.; Wang, C. H. *J. Chem. Phys.* **1993**, *98*, 3463–3468.
(22) (a) Wu, J. W. *J. Opt. Soc. Am. B* **1990**, *8*, 142–152. (b) Liu, L. Y.; Ramkrishna, D.; Lackritz, H. S. *Macromolecules* **1994**, *27*, 5987–5999.
(23) (a) Perez Belmonte, A.; Lopez Martinez, M. C.; Garcia de la Torre, J. *J. Phys. Chem.* **1991**, *95*, 952–955. (b) Dirk, C. W.; Devanathan, S.; Velez, M.; Chebremichael, F.; Kuzyk, M. G. *Macromolecules* **1994**, *27*, 6167–6176.
(24) Firestone, M. A.; Marks, T. J.; Ratner, M. A.; Lin, W.; Wong, G. K. *Macromolecules* **1995**, *28*, 2260–2269.
(25) Reference 7, pp 59–73.
(26) *Investigations on the Theory of the Brownian Movement*; Einstein, A., Ed.; Dover: New York, 1956.
(27) Chandrasekhar, S. *Rev. Mod. Phys.* **1943**, *15*, 1–21.
(28) *The Theory of Polymer Dynamics*; Doi, M., Edwards, S. F., Eds.; Oxford University Press: U.K., Oxford, 1988; pp 289–323.
(29) Ferry, J. D. *Viscoelastic Properties of Polymers*, 3rd ed.; J. Wiley & Sons: New York, 1980; pp 289–290.
(30) McCrum, N. G.; Read, B. E.; Williams, G. *Anelastic and Dielectric Effects in Polymeric Solids*, 1st ed.; Dover Publications: New York, 1991; pp 415.
(31) Roberts, G. E.; White, E. F. T. In *The Physics of Glassy Polymers*; Wiley: New York, 1973; pp 152–222.
(32) (a) Patashinsky, A. Z.; Ratner, M. A. *J. Chem. Phys.* **1994**, *101*, 6330–6339. See also: (b) Blumen, A., Ed. *Disorder Effects on Relaxation Processes*; Springer Verlag: Berlin, 1994. (c) Oppenheim, I., Shuler, K. E., Weiss, C. H., Eds. *Stochastic Processes in Chemical Physics*; MIT Press: Cambridge, 1971. (d) Sengupta, A.; Fayer, M. D. *J. Chem. Phys.* **1994**, *100*, 1672–1683. (e) Klafter, J. K.; Drake, J. M. In *Dynamics and Mechanisms of Photoinduced Transfer*; Mataya, N., Okada, T., Masuhara, H., Eds.; Elsevier: Amsterdam, 1992; pp 345–361.
(33) Brawer, S. *Relaxation in Viscous Liquids and Glasses*; American Ceramic Society; Columbus, OH, 1985; pp 42–43.
(34) Laidler, K. J.; Meiser, J. H. *Physical Chemistry*; Benjamin/Cummings: Menlo Park, CA, 1982; pp 380–381.
(35) Mortimer, R. G. *Mathematics for Physical Chemistry*; Macmillan Publishing Co., Inc.: New York, 1981; pp 124–125.
(36) Robin, P.; LeBarny, P.; Broussoux, D.; Pocholle, J. P.; Lemoine, V. In ref 8, pp 481–488.
(37) Boyd, G. T.; Francis, J. E.; Ender, D. A. *J. Opt. Soc. Am. B* **1991**, *8*, 887–894.
(38) Kuzyk, M. G.; Moore, R. C.; King, L. A. *J. Opt. Soc. Am. B* **1990**, *7*, 64–72.
(39) Dumont, M.; Levy, Y.; Morichere, D. In ref 8, pp 461–480.
(40) Hayashi, A.; Goto, Y.; Nakayama, M.; Kaluzynski, K.; Sato, H.; Kato, K.; Kondo, K.; Watanabe, T.; Miyata, S. *Chem. Mater.* **1992**, *4*, 555–562.
(41) Robello, D. R.; Dao, P. T.; Phelan, J.; Revelli, J.; Schildkraut, J. S.; Scozzafava, M.; Ulman, A.; Willand, C. S. *Chem. Mater.* **1992**, *4*, 425–435.
(42) Rondou, P.; VanBeylen, M.; Samyr, C.; S'heeven, G.; Persoons, A. *Makromol. Chem.* **1992**, *193*, 3045–3055.
(43) Loucif-Saibi, R.; Nakatomi, K.; Delaire, J. A.; Dumont, M.; Sekkat, Z. *Chem. Mater.* **1993**, *5*, 229–236.
(44) Firestone, M. A.; Lin, W.; Wong, G. K.; Ratner, M. A.; Marks, T. J. Manuscript in preparation.
(45) McConnell, J. *Rotational Brownian Motion and Dielectric Theory*; Academic Press: New York, 1980; pp 1–8.
(46) Arfken, G. *Mathematical Methods for Physicists*, 3rd ed.; Academic Press: New York, 1985; p 648.
(47) Bateman, H. *Partial Differential Equations of Mathematical Physics*; Cambridge University Press: New York, 1969; pp 363.
(48) Courant, R.; Hilbert, D. *Methods of Mathematical Physics*; John Wiley & Sons: New York, 1989; Vol. 1, pp 82–86.
(49) Zare, R. N. *Angular Momentum. Understanding Spatial Aspects in Chemistry and Physics*; John Wiley & Sons: New York, 1988; pp 48–63.
(50) Dhinojwala, A.; Wong, G. K.; Torkelson, J. M. *Macromolecules* **1993**, *26*, 5943–5953.
(51) Walsh, C. A.; Burland, D. M.; Lee, V. Y.; Miller, R. D.; Smith, B. A.; Twieg, R. J.; Volksen, W. *Macromolecules* **1993**, *26*, 3720–3722.
(52) Stanley, M.; McDonell, D. G.; Day, S. E. In *Organic Materials for Nonlinear Optics III*, Ashwell, G. J., Bloor, D., Eds.; Royal Society of Chemistry: Cambridge, U.K., 1993; pp 175–181.
(53) Rossler, E.; Sillescu, B. *A Comprehensive Treatment: Glass and Amorphous Materials*; VCH: Weinheim, 1991; Vol. 9, pp 574–615.
(54) Chow, T. S. *Adv. Polym. Sci.* **1992**, *103*, 149–190.
(55) Cohen, M. H.; Grest, G. S. *Phys. Rev. B* **1979**, *20*, 1077–1098.
(56) Williams, M. L.; Landel, R. F.; Ferry, J. D. *J. Am. Chem. Soc.* **1955**, *77*, 3701–3707.
(57) Eisenbach, C. D. *Ber. Bunsen-Ges. Chem.* **1980**, *84*, 680–690.
(58) Ferry, J. D. *J. Appl. Phys.* **1953**, *24*, 911–915.
(59) Williams, G. *J. Non-Cryst. Solids* **1991**, *131–133*, 1–12.
(60) Schaefer, J.; Sefcik, M. D.; Stejskal, E. O.; McKay, R. A.; Dixon, W. T.; Cais, R. E. *Macromolecules* **1984**, *17*, 1107–1118.
(61) Monnerie, L. In *Molecular Dynamics and Relaxation Phenomena in Glasses*, 1st ed.; Dorfmuller, T., Williams, G., Eds.; Springer-Verlag: New York, 1987; pp 125–143.
(62) Spiess, H. W. *Colloid Polym. Sci.* **1983**, *261*, 193–209.
(63) Man, H.-T.; Hyun, H. N. *Adv. Mater.* **1992**, *4*, 159–167.
(64) McCall, D. W.; In *Molecular Dynamics and Structure of Solids*; Carter, R., Rush, J., Eds.; National Bureau of Standards: Washington, DC, 1969; Vol. 301, pp 475–537.
(65) Valley, J. F.; Wu, J. W. *SPIE* **1990**, *1337*, 226–233.
(66) Meyrueix, R.; Mignani, G.; Tapolsky, G. In ref 8, pp 161–176.
(67) Meyrueix, R.; Lecomte, J. P.; Taplosky, G. *Nonlinear Opt.* **1991**, *1*, 201–211.
(68) For some representative examples, see: (a) Crumpler, E. T.; Reznichenko, J. L.; Li, D.; Marks, T. J.; Lin, W.; Lundquist, P.; Wong, G. K. *Chem. Mater.* **1995**, *7*, 596–598. (b) Ye, C.; Marks, T. J.; Yang, J.; Wong, G. K. *Macromolecules* **1987**, *20*, 2322–2324. (c) Hubbard, M. A.; Minami, N.; Ye, C.; Marks, T. J.; Wong, G. K. *Proc. SPIE—Int. Soc. Opt. Eng.* **1988**, *971*, 136–143. (d) Hubbard, M. A.; Marks, T. J.; Lin, W.; Wong, G. K. *Chem. Mater.* **1992**, *4*, 965–968. (e) Jin, Y.; Carr, S. H.; Marks, T. J.; Lin, W.; Wong, G. K. *Chem. Mater.* **1992**, *4*, 963–968. (f) Wang, J.-F.; Hubbard, M. A.; Jin, Y.; Lin, J. T.; Marks, T. J.; Lin, W. P.; Wong, G. K. *Proc. SPIE—Int. Soc. Opt. Eng.* **1993**, *2025*, 62–68. (g) Xu, C.; Wu, B.; Todorova, O.; Dalton, L. R.; Shi, Y.; Ranon, P.; Steier, W. H. *Macromolecules* **1993**, *26*, 5303–5309 and references therein. (h) Peng, Z.; Yu, L. *Macromolecules* **1994**, *27*, 2638–2640.
(69) Bussell, S. J.; Koch, D. A.; Hammer, D. A. *Biophys. J.* **1995**, *68*, 1836–1849.

MA9501205